Frontiers in Bioscience Landmark

*Front. Biosci. (Landmark Ed)* **2025**; 30(12): 46747
https://doi.org/10.31083/FBL46747

*Original Research*

# Eupatorin as a Promising Natural Compound Against Knee Osteoarthritis: From Network Pharmacology to Experimental Validation

Min-Jun Zhao[1,2,3,4,†], Jian-Li Yin[1,2,3,4,†], Jia-Hui Luo[1,2,3,4], Yang-Shuo Ge[1,3,4], Chun-Meng Huang[1,3,4], Ting-Ting Meng[1,3,4], Yu-Qing Zhai[1,3,4], Xin-Hui Huang[1,3,4], Liao-Lin Chen[1,3,4], Jia-Wei Du[1,3], Xu-Bo Wu[1,2,*], Dao-Fang Ding[1,3,4,*]

[1]Department of Rehabilitation Therapy, The Second Rehabilitation Hospital of Shanghai, 200441 Shanghai, China
[2]Department of Rehabilitation Medicine, Shanghai Pudong New Area People's Hospital, 201299 Shanghai, China
[3]Institute of Rehabilitation Medicine, Shanghai Academy of Traditional Chinese Medicine, 201203 Shanghai, China
[4]School of Rehabilitation Science, Shanghai University of Traditional Chinese Medicine, 201203 Shanghai, China
*Correspondence: Wuxubo320@163.com (Xu-Bo Wu); dingdaofang@shutcm.edu.cn (Dao-Fang Ding)
[†]These authors contributed equally.
Academic Editors: Kota V. Ramana and Elisa Belluzzi
Submitted: 19 September 2025 Revised: 24 November 2025 Accepted: 30 November 2025 Published: 22 December 2025

**Abstract**

**Background**: Knee osteoarthritis (KOA), a chronic degenerative joint disease, is primarily driven by inflammation-induced cartilage degradation, which represents its core pathological feature. Eupatorin, with its distinct anti-inflammatory properties, has emerged as a promising candidate for KOA research. This study aimed to explore the therapeutic potential of Eupatorin and elucidate its underlying mechanisms in KOA through an integration of network pharmacology analysis and experimental validation. **Methods**: Potential targets of Eupatorin and KOA-related genes were retrieved from multiple databases, and the overlapping targets were utilized to build a protein–protein interaction (PPI) network to identify core targets. Gene Ontology (GO) and Kyoto Encyclopedia of Genes and Genomes (KEGG) enrichment analyses were performed to characterize the associated biological processes (BP), molecular functions (MF), and cellular components (CC). Additionally, molecular docking was performed to assess the binding affinities of Eupatorin with the core targets. Direct target engagement was confirmed using a cellular thermal shift assay (CETSA). Finally, biological experiments using interleukin-1$\beta$ (IL-1$\beta$)-stimulated primary *rat* chondrocytes were carried out to validate the protective effects of Eupatorin through its anti-inflammatory activity. **Results**: Network pharmacology analysis revealed 46 overlapping targets, with Matrix Metallopeptidase 9 (MMP9), Epidermal Growth Factor Receptor (EGFR), and Prostaglandin G/H synthase 2 (PTGS2) as key nodes within the PPI network. GO and KEGG enrichment analyses revealed significant associations with inflammatory responses and extracellular matrix (ECM) metabolism, particularly the phosphatidylinositol 3-kinase (PI3K)/protein kinase B (AKT) and estrogen signalling pathways. Molecular docking further confirmed strong binding affinities between Eupatorin and key targets, including MMP9, EGFR, and PTGS2. CETSA validated the direct binding of Eupatorin to PTGS2. Eupatorin significantly inhibited IL-1$\beta$-induced cytokine expression and ECM degradation while promoting ECM synthesis and restoring impaired autophagy in inflamed chondrocytes, as indicated; however, no significant effect on cellular senescence was observed. Mechanistically, Eupatorin exerted its protective effects on chondrocytes by attenuating the upregulation of the PI3K/AKT and estrogen signalling pathways. **Conclusion**: Eupatorin has demonstrated potential for use in KOA therapy by targeting inflammation and ECM, and by regulating the PI3K/AKT and estrogen-associated signaling pathways.

**Keywords:** Eupatorin; knee osteoarthritis; network pharmacology; chondrocytes; inflammation; extracellular matrix

## 1. Introduction

Osteoarthritis (OA) represents a widespread degenerative disorder of the entire joint that impairs all articular tissues [1]. Pathologically, OA involves not only articular cartilage degeneration but also changes such as meniscal tears, inflammation/fibrosis of the infrapatellar fat pad, and synovial hyperplasia with fibrosis [2,3]. Knee osteoarthritis (KOA) is the most common subtype of OA, with its primary features being progressive articular cartilage degeneration and secondary subchondral bone remodelling [4]. The pathogenesis of KOA is multifactorial and involves complex interactions among mechanical, biochemical, and inflammatory factors that collectively drive a series of pathological alterations in the articular cartilage, including fibrillation, fissures, ulceration, and wear [5]. In the treatment of KOA, anti-inflammatory therapy has long been considered a cornerstone strategy for alleviating pain and improving joint mobility [6]. Although emerging approaches such as stem cell therapy and ADAMTS-5 inhibition have shown considerable promise, significant challenges remain, including the risk of infection, limited capacity to restore cartilage thickness, and the potential for aberrant tissue overgrowth [7–10]. These limitations un-

derscore the need to further explore and validate novel therapeutic targets for treating KOA [11].

Cartilage degradation is a hallmark of KOA, during which chondrocytes attempt to homeostasis by maintaining a balance of anabolic and catabolic processes [12,13]. As key local sources of inflammatory factors, synovial tissue and the infrapatellar fat pad (IFP) can synergistically secrete proinflammatory cytokines including interleukin-1$\beta$ (IL-1$\beta$), interleukin-6 (IL-6), and tumour necrosis factor-$\alpha$ (TNF-$\alpha$), which induce metabolic disturbances that disrupt the extracellular matrix (ECM) homeostasis of cartilage, thus exacerbating tissue damage and driving disease progression [14,15]. These inflammatory factors may further amplify the inflammatory cascade by aberrantly activating the MAPK and NF-$\kappa$B signalling pathways [16]. Notably, the phosphatidylinositol 3-kinase (PI3K)/protein kinase B (AKT) pathway modulates inflammatory responses through the regulation of multiple key effector molecules, including NF-$\kappa$B, underscoring the critical need to develop novel therapeutic agents that specifically target these inflammatory signalling pathways and their downstream effectors [17].

Eupatorin (3′,5-dihydroxy-4′,6,7-trimethoxyflavone) is a natural flavonoid compound predominantly isolated from diverse medicinal plants, including Isatis indigotica fortune, Pratia nummularia, and members of the *Eupatorium genus* [18]. This compound was shown to display anti-inflammatory properties, primarily by suppressing the secretion of inflammatory mediators through the inhibition of key signalling pathways such as STAT1 and NF-$\kappa$B in lipopolysaccharide (LPS)-exposed RAW 264.7 cells and a mouse model of carrageenan-induced paw oedema inflammation [19,20]. The systemic administration of Eupatorin significantly decreased serum concentrations of TNF-$\alpha$ and IL-1$\beta$ in a murine breast cancer model, concomitantly attenuating the activity of the NF-$\kappa$B pathway, which in turn inhibited the epithelial-to-mesenchymal transition of tumour cells [21]. Additionally, González-Cortazar *et al*. [22] reported that Eupatorin isolated from Salvia lavanduloides extracts inhibited ear oedema inflammation by 72% in *mice*.

Given that inflammation is a critical driver of the onset and progression of KOA, and that Eupatorin has been demonstrated to exert robust anti-inflammatory properties in diverse disease models, we aimed to investigate its potential protective role in cartilage under inflammatory conditions. Herein, we initially utilized network pharmacology and molecular docking to systematically screen the potential molecular targets and key signalling pathways through which Eupatorin may exert its therapeutic effects in KOA. We then established an IL-1$\beta$-induced inflammatory chondrocyte model to assess the anti-inflammatory efficacy of Eupatorin. Finally, we integrated the experimental results with network pharmacology predictions to illustrate the molecular mechanisms underlying Eupatorin's cartilage-protective effects in KOA. The overall study design is illustrated in Fig. 1.

## 2. Materials and Methods

### *2.1 Network Pharmacology*

#### 2.1.1 Identification of Eupatorin-Associated Genes

The core targets of Eupatorin were initially screened using the Traditional Chinese Medicine Systems Pharmacology Database (TCMSP 2.0; https://www.tcmsp-e.com/load_intro.php?id=43) [23]. The corresponding SMILES identifier for Eupatorin was retrieved from the PubChem database (https://pubchem.ncbi.nlm.nih.gov) [24] and subsequently entered into the Swiss Target Prediction platform (http://swisstargetprediction.ch/) to predict potential targets, and only targets with a probability greater than zero were retained [25]. All of the predicted targets were normalized by converting their protein names to official gene symbols via the UniProt database (https://www.uniprot.org/) [26]. After removing duplicate entries, a list of potential target genes for Eupatorin was constructed.

#### 2.1.2 Collection of KOA-Associated Genes

The Medical Subject Headings (MeSH) terms "Knee Osteoarthritis" and "Osteoarthritis, Knee" were used to search for disease-associated target genes across multiple databases, including DisGeNET (https://www.disgenet.org/), GeneCards (https://www.genecards.org/), Online Mendelian Inheritance in Man (OMIM; https://omim.org/), and the Therapeutic Target Database (TTD; http://db.idrblab.net/ttd/). The obtained gene targets were subsequently normalized and converted into matching UniProt IDs through the UniProt database (https://www.uniprot.org/). Finally, R software (Version 4.4.2, R Core Team 2024, R Foundation for Statistical Computing, Vienna, Austria. Available from: https://www.R-project.org/) and the "Venn diagram" package were applied to identify the overlap of genes between Eupatorin-targeted genes and KOA-related genes, and a Venn diagram was generated.

#### 2.1.3 Construction and Analysis of a PPI Network

The intersecting targets of Eupatorin and KOA were submitted to the STRING database (https://string-db.org), where the organism was specified as *Homo sapiens* and a medium confidence score was set as the minimum interaction threshold. Upon completion of the analysis, the resulting interaction data were exported in TSV format for downstream processing. A PPI network was subsequently constructed with Cytoscape (Version 3.9.1, Institute for Systems Biology, Seattle, WA, USA, Available from: https://www.cytoscape.org/). To enhance the comprehensiveness and accuracy of the network analysis, we employed two Cytoscape plugins, CytoNCA and CytoHubba [27,28]. Using CytoNCA, centrality metrics for

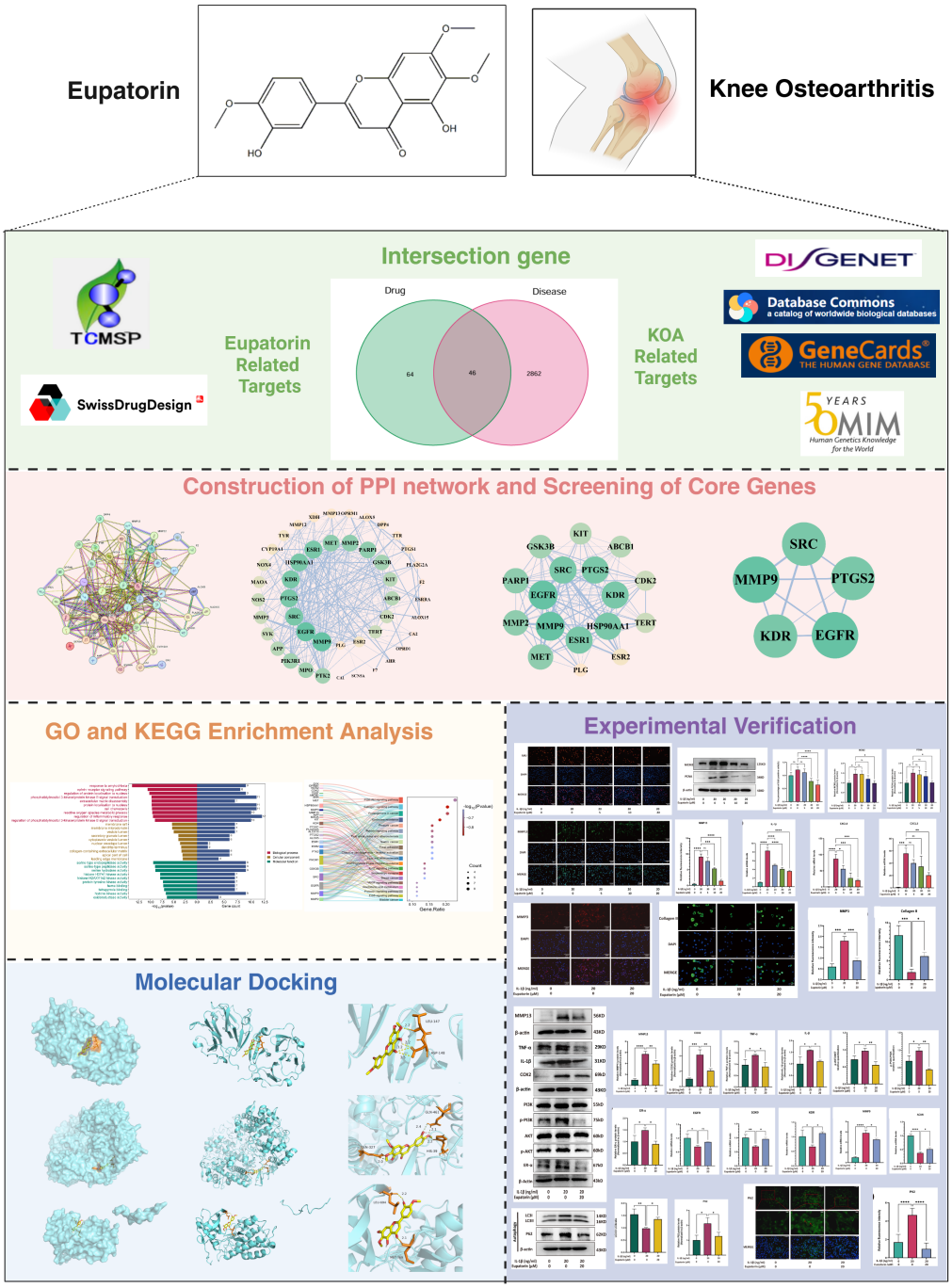


**Fig. 1. Flowchart of this study.** Created at https://BioRender.com.

each node (including degree, betweenness centrality, and closeness centrality) were calculated to evaluate node importance within the network. Nodes with degree, betweenness centrality, and closeness centrality values exceeding the respective median thresholds were retained through two successive rounds of filtering to identify core targets. In parallel, CytoHubba was used to predict key genes and subnetworks on the basis of the maximal clique centrality (MCC) algorithm. During visualization, node size was scaled proportionally to its degree value (larger nodes indicating higher degrees), and node colour intensity reflected target influence (darker colours indicating greater influence).

### 2.1.4 GO and KEGG Enrichment Analysis

For the purpose of further investigating the potential biological roles of the identified targets, using the R package "ClusterProfiler", we conducted Gene Ontology (GO) enrichment analysis, including the three subcategories of biological process (BP), molecular function (MF), and cel-

lular component (CC) subcategories, along with Kyoto Encyclopedia of Genes and Genomes (KEGG) pathway analysis [29]. Specifically, enrichment terms were filtered on the basis of *p* values, and the top 10 significant GO terms and the top 20 significant KEGG pathways were selected for in-depth analysis. Finally, the results were visualized as bar charts and Sankey diagrams using an online bioinformatics platform to intuitively demonstrate the distribution and proportional flow of intersecting genes across different pathways (http://www.bioinformatics.com.cn/).

### *2.2 Molecular Docking*

The 2D chemical structure file (SDF format) of Eupatorin was downloaded from the PubChem database (https://pubchem.ncbi.nlm.nih.gov). The minimum binding energy conformation of Eupatorin was calculated using ChemBio3D version 22.0.0.22 and saved in MOL2 format. Three-dimensional structures of the core target proteins Matrix Metallopeptidase 9 (MMP9) (PBD code: 1ITV), EGFR (PBD code: 2XKN), and PTGS2 (PBD code: 3OLT) were downloaded from the Protein Data Bank (PDB; https://www.rcsb.org). All protein structures underwent preparation through the removal of solvents and organics using PyMOL (Version 3.1, Schrödinger., New York, NY, USA, Available from: https://pymol.org/). The protein receptor grid box files were generated with AutoDockTools (Version 1.5.7, Scripps Research, La Jolla, CA, USA. Available from: https://ccsb.scripps.edu/), and molecular docking between Eupatorin and individual target proteins was carried out with AutoDock Vina. All the docking run options were default parameters (exhaustiveness = 10, num_modes = 20, and energy range = 5.0 kcal/mol). Finally, the binding patterns and key intermolecular interactions of candidate active compounds with core target proteins were evaluated and visualized in PyMOL version 4.6.0.

### *2.3 Isolation and Culture of Primary Chondrocytes*

One-day-old *Sprague–Dawley (SD) rats* (Shanghai Sipur-Bikai Laboratory Animal Co., Ltd. [Certificate No. SCXK (Shanghai) 2018-0006] licence no. SCXK (Shanghai) 20180006) were euthanized by inhalation of an overdose of isoflurane (at a concentration of 5%) and immediately immersed in 75% ethanol for 10 minutes. Subsequent to three consecutive washes using phosphate-buffered saline (PBS), all the procedures were performed under sterile conditions. Articular cartilage was carefully harvested from the tibial and femoral condyles and rinsed extensively with PBS. Cartilage tissues were minced into approximately 1 $mm^3$ fragments and transferred into 0.5% type II collagenase solution (SigmaAldrich, C6885, St. Louis, MO, USA) for enzymatic digestion at 37 °C with gentle agitation (150 rpm) for 60 minutes. The digestion mixture was subsequently harvested and subjected to centrifugation at 1500 ×g for 5 minutes, after which the supernatant was removed. The cell pellet was resuspended in Dulbecco's modified Eagle's medium with high glucose (DMEM; Biosera, LMD1110/500, Cholet, Maine-et-Loire, France) supplemented with 10% fetal bovine serum (FBS, Biosera, FB-1058) and 1% penicillin–streptomycin (Beyotime, C0222, Shanghai, China) and seeded into 10 cm culture dishes. The cells were cultured at 37 °C in a humidified incubator containing 5% $CO_2$. All primary cells were validated for their identity by type II collagen immunofluorescence staining (see **Supplementary Fig. 1** for detailed results).

### *2.4 Cell Viability Assay*

Primary chondrocytes were first plated into 96-well plates at a density $5 \times 10^3$ cells/well, with 100 µL of complete medium supplemented to each well, the plates were then cultured at 37 °C in a humidified 5% $CO_2$ incubator for 24 h to allow cell adhesion, after which cell viability was assessed using a Cell Counting Kit (CCK-8) (Biosharp, BS350B, Beijing, China).

Thereafter, the chondrocytes were treated with increasing concentrations of Eupatorin (TargetMol, T7032, Boston, MA, USA) (2, 5, 10, 20, and 50 µM). Simultaneously, blank wells (culture medium only) and vehicle control wells (equivalent volume of DMSO) were included. Following 24 and 48 h of culture, 10 µL of CCK-8 solution was added to every well prior to incubation for 1–4 h at 37 °C. The absorbance at 450 nm ($OD_{450}$) was detected with a microplate reader, after which the cell viability was computed using the following equation: cell viability (%) = (ODsample-ODblank)/(ODcontrol-ODblank) × 100%.

### *2.5 EdU Incorporation Assay*

In accordance with the manufacturer's instructions, chondrocyte proliferation was assessed via a 5-ethynyl-2′-deoxyuridine (EdU) incorporation assay (BeyoClick™ EdU Cell Proliferation Kit with AF555, Beyotime, C0075). Briefly, cells were seeded in 24-well plates at $1 \times 10^5$ cells/well and allowed to reach 70–80% confluence. Five groups were established by randomly dividing the cells, including: (1) the non-intervened group, which included untreated chondrocytes; (2) the model group, in which chondrocytes were stimulated with IL-1$\beta$ (Bio-Techne, 501-RL, Minneapolis, MN, USA) (20 ng/mL) for 24 h to induce an inflammatory phenotype; and (3–5) the experimental groups, in which Eupatorin (5, 10, or 20 µM) was added to the IL-1$\beta$-treated chondrocytes. Following treatment, the cells were exposed to EdU (10 µM) for 2 h, fixed with Immunol Staining Fix Solution (Beyotime, P0098) and permeabilized with 0.5% Triton X-100 (Beyotime, P0106). The EdU signal was visualized using the Click-iT™ reaction cocktail according to the kit protocol, and the nuclei were counterstained with DAPI (Proteintech, CM07245, Rosemont, IL, USA). Images were captured with a fluorescence microscope (Olympus, IX73, Hachioji, Tokyo, Japan), and

the percentage of EdU-positive cells was used as an indicator of proliferation (EdU-positive cell count/total cell count) $\times$ 100%.

### *2.6 Experimental Grouping*

Primary articular chondrocytes were assigned to three groups: the non-intervened group (untreated), the model group (20 ng/mL IL-1$\beta$ (Bio-Techne, 501-RL), and the Eupatorin (TargetMol, T7032) group (20 ng/mL IL-1$\beta$ + 5, 10, or 20 µM Eupatorin). Primary articular chondrocytes were co-treated concurrently with IL-1$\beta$ and Eupatorin for 24 hours, and on the basis of comprehensive evaluations of cell viability and catabolic factor expression, 20 µM was determined as the optimal treatment concentration. Immunofluorescence (IF), real-time quantitative PCR (RT–qPCR), and Western blotting (WB) were subsequently employed to investigate the anti-inflammatory functions and underlying mechanisms of Eupatorin at this concentration.

### *2.7 Reverse Transcription–Quantitative Polymerase Chain Reaction*

Total RNA was isolated from chondrocytes of each experimental group using the RNAeasy™ Animal RNA Isolation Kit (column-based) (Beyotime, R0024) in accordance with the manufacturer's instructions. Complementary DNA (cDNA) was synthesized via the Evo MMLV Reverse Transcription Kit (Accurate Biotechnology, AG11706, Hunan, China). qPCR was performed with the SYBR® Green Pro Taq HS Premix qPCR Kit (Accurate Biotechnology, AG11746) in a 20 µL reaction system comprising10 µL of SYBR Green Pro Taq HS Premix IV, 1 µL of forward and reverse primers (each), 5 µL of cDNA template, and 4 µL of RNase-free water. PCRs were performed on a QuantStudio 5 real-time PCR system (Applied Biosystems, Foster City, CA, USA). Relative mRNA expression levels were calculated using the $2^{-\Delta\Delta Ct}$ method. qPCR primer sequences are provided in detail in Table 1.

**Table 1. Primer Sequences used for RT–qPCR.**

| Gene | Primer Sequence (5′-3′) | Product Length (bp) |
|---|---|---|
| *β-Actin* | Forward: GCTACAGCTTCACCACCACA<br>Reverse: GCCATCTCTTGCTCGAAGTC | 94 |
| *IL-1β* | Forward: GACTTCACCATGGAACCCGT<br>Reverse: GGAGACTGCCCATTCTCGAC | 104 |
| *CXCL3* | Forward: ACCAGCCTTCAGGGACTGT<br>Reverse: GGCTATGACTTCTGTCTGGGT | 140 |
| *CXCL6* | Forward: TTCTGCTGCTGTTCACACTG<br>Reverse: TATCAACGGAGCTTGTGGGT | 233 |
| *MMP9* | Forward: GATCCCCAGAGCGTTACTCG<br>Reverse: GTTGTGGAAACTCACACGCC | 132 |
| *SOX9* | Forward: CAGACCAGTACCCGCATCTG<br>Reverse: GCTCTCGTTCAGCAGTCTCC | 77 |
| *ACAN* | Forward: GCCTCTCAAGCCCTTGTCTG<br>Reverse: GATCTCACACAGGTCCCCTC | 101 |
| *EGFR* | Forward: CCTATGGGCCAAAGATCCCA<br>Reverse: CCTTGATGGCCACAGGATTT | 324 |
| *KDR* | Forward: CAGCTCGTCATCCTAGAGCG<br>Reverse: GTTAGGTTCCGGTTCCCGTC | 197 |

*IL-1β*, interleukin-1β; *CXCL3*, C-X-C chemokine ligand 3; *CXCL6*, C-X-C chemokine ligand 6; *MMP9*, Matrix Metallopeptidase 9; *SOX9*, SRY-box transcription factor 9; *ACAN*, Aggrecan; *EGFR*, Epidermal Growth Factor Receptor; *KDR*, Kinase Insert Domain Receptor.

### *2.8 Western Blot Analysis*

Total protein was extracted from chondrocytes using RIPA lysis buffer (Servicebio, G2002, Wuhan, China) supplemented with a phosphorylated protease inhibitor (Servicebio, G2007) and a serine protease inhibitor (PMSF, Servicebio, G2008). After determining protein concentration via a BCA protein assay kit (Thermo Fisher Scientific, 23225, Waltham, MA, USA), 10 µg of protein sample was subjected to electrophoresis separation using the Omni-Easy™ One-step Colour PAGE Gel Rapid Preparation Kit (Epizyme Biotech, PG212, Cambridge, MA, USA). The separated proteins were subsequently transferred from the gel to a PVDF membrane (MerckMillipore, IPVH00010, Darmstadt, Hesse, Germany) and blocked with a rapid blocking solution (Epizyme Biotech, PS108P) to prevent nonspecific binding sites. Next, the membrane was incubated overnight with primary antibodies at 4 °C including: $\beta$-actin (Beyotime, AF0003, 1:2000), PCNA (Santa Cruz, sc-71858, 1:2000, Dallas, TX, USA), MCM2 (Selleck, F0581, 1:2000, Houston, TX, USA), TNF-$\alpha$ (Santa Cruz, sc-52746, 1:2000), MMP13 (Beyotime, AF7479, 1:2000), COX2 (Selleck, F0327, 1:2000), PI3K (Cell Signaling Technology, #4292, 1:2000, Danvers, MA, USA), phospho-PI3K (Cell Signaling Technology, #4228, 1:2000), AKT (Cell Signaling Technology, #4614, 1:2000), phospho-AKT (p-AKT) (Cell Signaling Technology, #4060, 1:2000), P62 (Beyotime, AF0279, 1:2000), and LC3 (Beyotime, AF5225, 1:2000). The membrane was removed the next day and subsequently incubated with peroxidase-conjugated secondary antibodies, including anti-mouse IgG, HRP-linked antibody (Cell Signaling Technology, #7076, 1:7000), anti-rabbit IgG and HRP-linked antibody (Cell Signaling Technology, #7074, 1:7000). Finally, the results were visualized using a chemiluminescence imaging analyser (Bio-Rad, ChemiDoc, Hercules, CA, USA), and the protein bands were quantitatively analysed using ImageJ software (Version 1.53t, National Institutes of Health, MD, USA. Available from: https://imagej.net/ij/). $\beta$-actin was employed as a loading control for quantifying the expression levels of other proteins.

### *2.9 Immunofluorescence (IF) Assay*

Chondrocytes were fixed with Immunol Staining Fix Solution (Beyotime, P0098) for 10 minutes. Thereafter, the

cells were subjected to permeabilization with 0.5% Triton X-100 and rinsed three times with PBS. The samples were then blocked with immunostaining blocking buffer (Beyotime, P0102) for 1 hour at room temperature to reduce nonspecific binding. Afterwards, the cells were incubated with primary antibodies targeting collagen II (Santa Cruz, sc52658), MMP13 (Santa Cruz, sc-30073) and MMP3 (Santa Cruz, sc21732) overnight at 4 °C, and both were diluted 1:500. The following day, the unbound primary antibodies were removed by washing the cells three times with PBST. The cells were then incubated with the appropriate fluorescently labelled secondary antibodies, namely, goat anti-rabbit IgG (H+L) cross-adsorbed secondary antibody, Alexa Fluor™ 488 (Thermo Fisher Technology, A11008, Waltham, MA, USA), Alexa Fluor® 488-conjugated goat anti-mouse IgG (H+L) (Servicebio, GB25301), goat anti-rabbit IgG (H+L) cross-adsorbed secondary antibody, and Alexa Fluor™ 555 (Thermo Fisher Technology, A21428) (diluted 1:1000), for 1 hour at room temperature. Afterwards, the nuclei were counterstained with DAPI (Proteintech, CM07245) for 10 minutes at room temperature to facilitate nuclear localization. Finally, the samples were washed three times with PBST in the dark to remove any unbound secondary antibody and excess DAPI. Fluorescence images were acquired with a digital inverted fluorescence microscope (Olympus, IX73). The mean fluorescence intensities were quantified across six randomly selected fields per sample using ImageJ software to assess target protein expression levels.

### *2.10 Cellular Thermal Shift Assay (CETSA)*

Primary rate chondrocytes were cultured to 80–90% confluence, harvested, and resuspended in ice-cold PBS supplemented with 1% PMSF. Cells were treated with Eupatorin (20 µM, dissolved in DMSO) or vehicle (DMSO) at 37 °C for 1 h. Samples were heated in a metal heat block (45 °C, 50 °C, 55 °C, 60 °C, 65 °C, 70 °C, 3 min) and then cooled (liquid nitrogen, 3 min). The lysates were prepared via three freeze–thaw cycles, centrifuged (14,000 rpm, 15 min, 4 °C) to collect soluble fractions, and then subjected to Western blotting.

### *2.11 Statistical Analysis*

All statistical analyses and graphical visualizations were conducted with GraphPad Prism v10.0.0 for Windows (GraphPad Software, Boston, MA, USA; https://www.graphpad.com). One-way analysis of variance (ANOVA) was used to compare multiple groups, with subsequent Tukey's post hoc test for pairwise comparisons. Statistical significance was considered present when the $p$ value was $<0.05$. All experiments were conducted in triplicate, and data are expressed as the means ± SD of three independent experiments.

## 3. Results

### *3.1 Network Pharmacology Analysis Results*

#### 3.1.1 Prediction of Shared Targets Between Eupatorin and KOA

In total, 110 putative targets of Eupatorin were obtained from the TCMSP and Swiss Target Prediction databases. Specifically, the TCMSP database provided target information for 14 active Eupatorin-related compounds, whereas Swiss Target Prediction yielded 100 predicted targets. After removing duplicate entries, 110 unique targets remained (**Supplementary Table 1A**). Concurrently, 2908 KOA-associated targets were retrieved from four disease databases (Fig. 2a and **Supplementary Table 1B**). To elucidate the potential mechanisms by which Eupatorin may exert therapeutic effects in KOA, overlapping targets between Eupatorin and KOA were identified via R software, and a Venn diagram was generated (Fig. 2b). The analysis revealed 46 common targets that may play critical roles in the pharmacological action of Eupatorin against KOA.

#### 3.1.2 Construction of the PPI Network

To further identify potential targets of Eupatorin in KOA, the 46 overlapping targets were imported into the STRING database (https://string-db.org) with the organism restricted to *Homo sapiens* and a confidence score threshold of $> 0.4$ (Fig. 2c). A PPI network comprising 46 nodes and 286 edges was constructed and subsequently visualized using Cytoscape (Fig. 2d) (details of the connectivity rankings are shown in **Supplementary Table 2**). Centrality analysis was performed using the CytoNCA plugin in Cytoscape. During the first round of filtering, nodes meeting the following criteria were selected: degree centrality (DC) $>13$, betweenness centrality (BC) $>11.342$, and closeness centrality (CC) $>0.548$, resulting in 17 key targets (Fig. 2e). A second, more stringent screening of the resulting subnetwork employed thresholds of DC $>14$, BC $>3.15$, and CC $>0.888$, ultimately yielding five core targets including: MMP9, EGFR, PTGS2, KDR, and SRC, and we identified the top three hub genes (Table 2) (details of the centrality analysis are shown in **Supplementary Table 3**). Additionally, the Cytohubba plugin was used to predict and visualize important genes and subnetworks on the basis of the MCC algorithm (Fig. 2f).

#### 3.1.3 GO and KEGG Enrichment Analysis

To further elucidate the biological functions of Eupatorin in the treatment of KOA, functional enrichment analyses were performed. In total, 1466 GO terms were enriched, including 1285 BP, 33 CC, and 148 MF terms (**Supplementary Table 4**). The top-ranked enriched terms for each category are visualized in a histogram; Fig. 3a displays the top 10 enriched terms in each GO category. These results demonstrate that Eupatorin may be implicated in biological processes, including the inflammatory response, ECM catabolism, and reactive oxygen species metabolism.

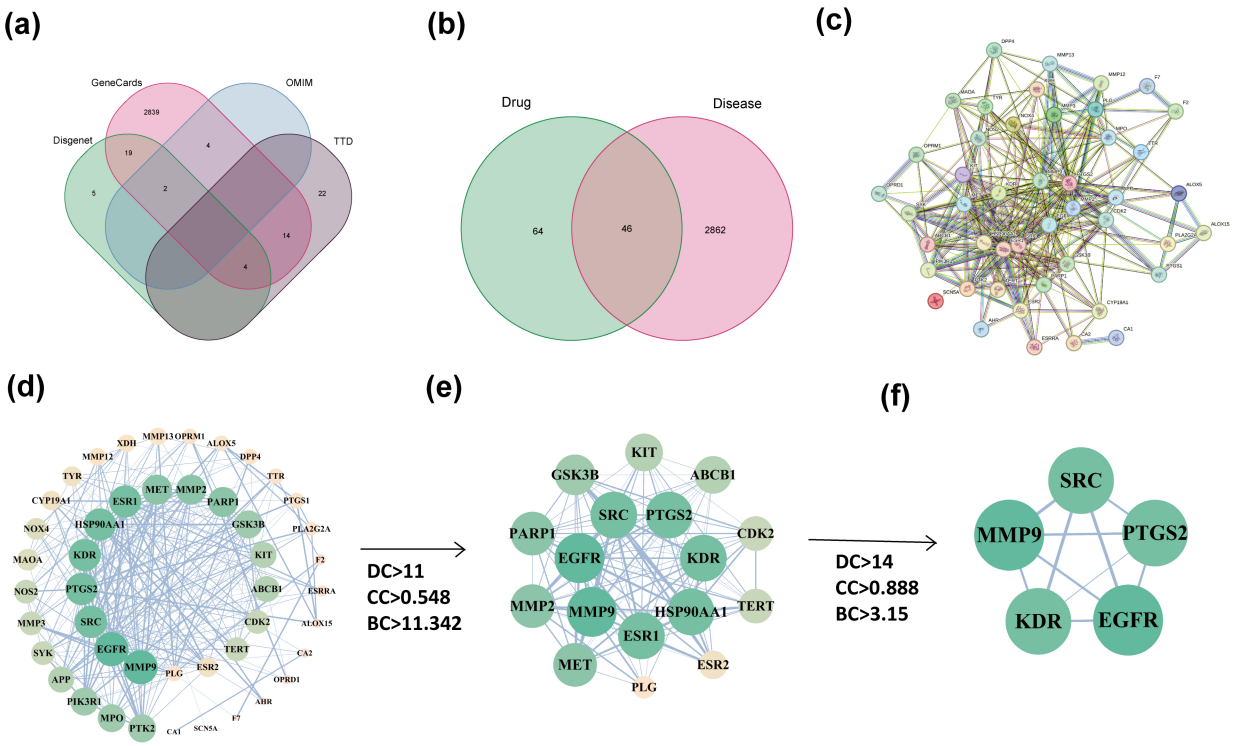


**Fig. 2. Construction of the target and PPI network of Eupatorin against KOA.** (a) Targets associated with KOA. (b) Venn diagram of overlapping genes between Eupatorin and KOA. (c) PPI network and identification of hub genes. (d) The initial and hub networks were constructed on the basis of the values of DC, CC and BC. (e) Top 17 hub genes. (f) Top 5 hub genes. The arrows indicate the process of screening for hub genes using the Cytohubba plugin. Disgenet, Disease Gene Network; OMIM, Online Mendelian Inheritance in Man; TTD, Therapeutic Target Database; DC, degree centrality; CC, closeness centrality; BC, betweenness centrality.

**Table 2. Information on the Core Targets in the PPI Network.**

| No. | UniProt ID | Gene Symbol | Protein name | BC | CC | DC |
|---|---|---|---|---|---|---|
| 1 | P14780 | MMP9 | Matrix metalloproteinase 9 | 230.799 | 0.762 | 31 |
| 2 | P00533 | EGFR | Epidermal growth factor receptor erbB1 | 160.349 | 0.737 | 30 |
| 3 | Q05769 | PTGS2 | Prostaglandin G/H synthase 2<br>Cyclooxygenase-2 | 263.268 | 0.762 | 32 |

DC, degree centrality (reflecting the node's direct connection ability); BC, betweenness centrality (measuring the node's mediating role in network paths); CC, closeness centrality (characterizing the node's proximity to other nodes).

For pathway analysis, the enrichment analysis of the 46 core genes revealed 80 significantly enriched pathways ($p < 0.05$) (**Supplementary Table 5**). On the basis of KEGG enrichment $p$ values, gene counts, and associated compound–target information, the top 20 pathways were selected and integrated into a gene–pathway association Sankey diagram (Fig. 3b). Notably, enrichment of the PI3K/AKT signalling pathway and the estrogen signalling pathway was high, suggesting that Eupatorin may exert its therapeutic effects in KOA through these key signalling cascades.

### 3.1.4 Interaction Between Eupatorin and Targets

On the basis of the identified compound–target relationships, molecular docking was performed between Eupatorin and the core targets MMP9, PTGS2 and EGFR, and in consideration of both the binding energy values and the centrality of these targets within the PPI network, MMP9, PTGS2, and EGFR were selected for detailed visualization (Fig. 4). Binding energy scores $\leq$–5.0 kcal/mol suggest favourable ligand–receptor interactions [30]. These results not only confirm the accuracy of our selected core targets but also highlight the potential therapeutic effects of Eupatorin in KOA treatment. We visually presented the docking of the core genes with small-molecule ligands and recorded the binding scores of each core gene in Table 3.

To further validate the binding interaction between Eupatorin and its highest-affinity target PTGS2 (also known as COX2; binding energy: –9.4 kcal/mol), we performed a CETSA. Compared with the DMSO control, Eu-

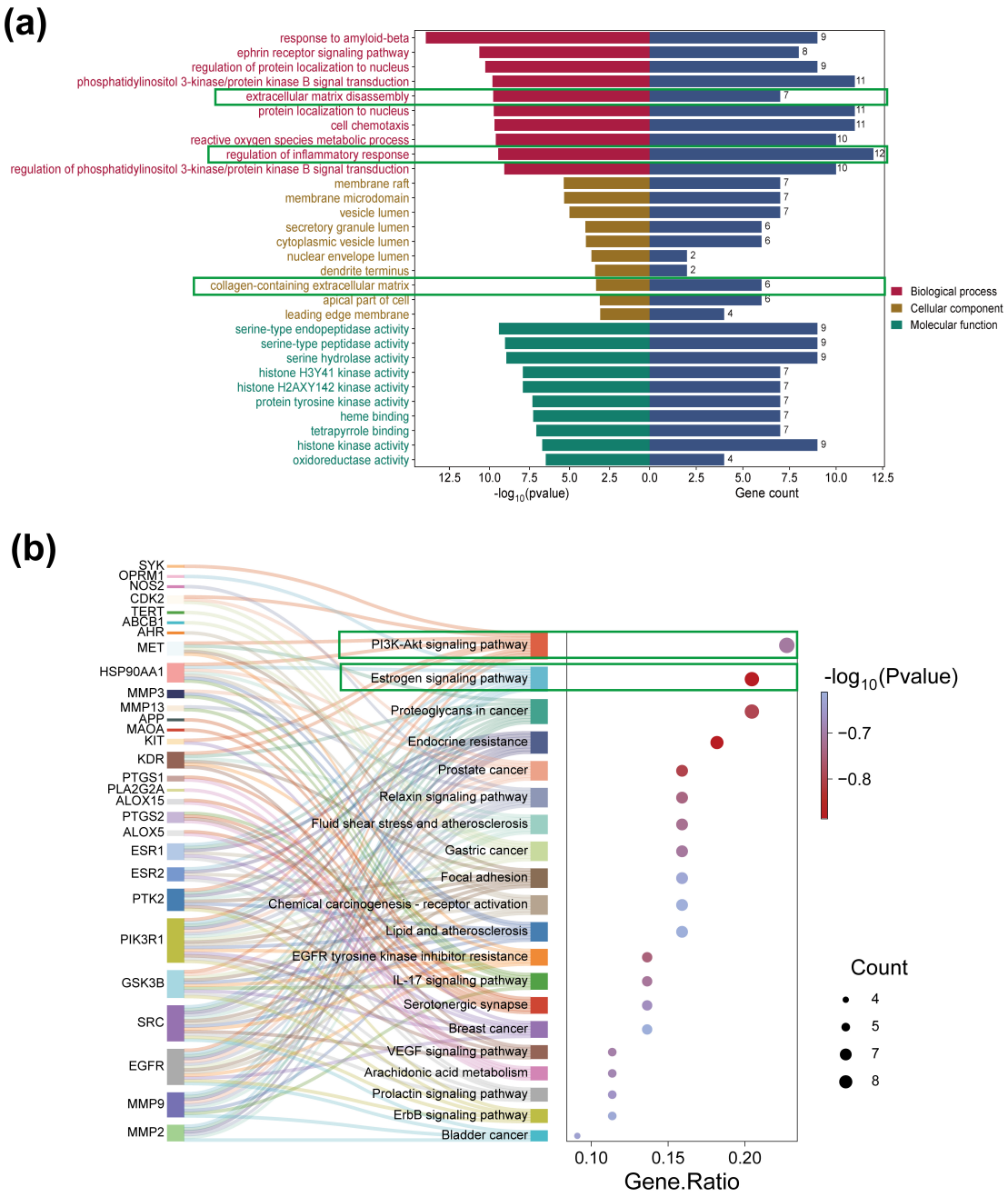


**Fig. 3. GO and KEGG analysis.** (a) Bar chart of GO analysis for the enrichment of 46 targets, including BP, CC, and MF. (b) Bubble plot and Sankey diagram of the results of the KEGG enrichment analysis for the 46 targets. GO, Gene Ontology; KEGG, Kyoto Encyclopedia of Genes and Genomes. Green boxes highlight the GO terms and KEGG pathways that were the focus of this study, which are hypothesized to be key mediators of Eupatorin's therapeutic effects on KOA.

patorin treatment (20 μM) increased the thermal stability of COX2 across the temperature range (Fig. 4d). These findings provide compelling evidence that Eupatorin directly targets COX2, a core target identified through integrated network pharmacology and molecular docking approaches.

### *3.2 Determining the Suitable Eupatorin Dose*

The results of the CCK-8 assay revealed that Eupatorin (≤20 μM) did not influence chondrocyte viability, whereas 50 μM Eupatorin significantly decreased cell viability ($p < 0.05$; Fig. 5a). Treatment for 48 h reduced chondrocyte viability by more than 40% across all the tested concentrations of Eupatorin (Fig. 5b). Therefore, to mitigate cytotoxicity risks and ensure stable cell function for subsequent assays, we standardized subsequent experiments to a 24-hour treatment period. Within the confirmed noncytotoxic concentration window (≤20 μM), we selected three stepwise doses—low (5 μM), medium (10 μM), and high

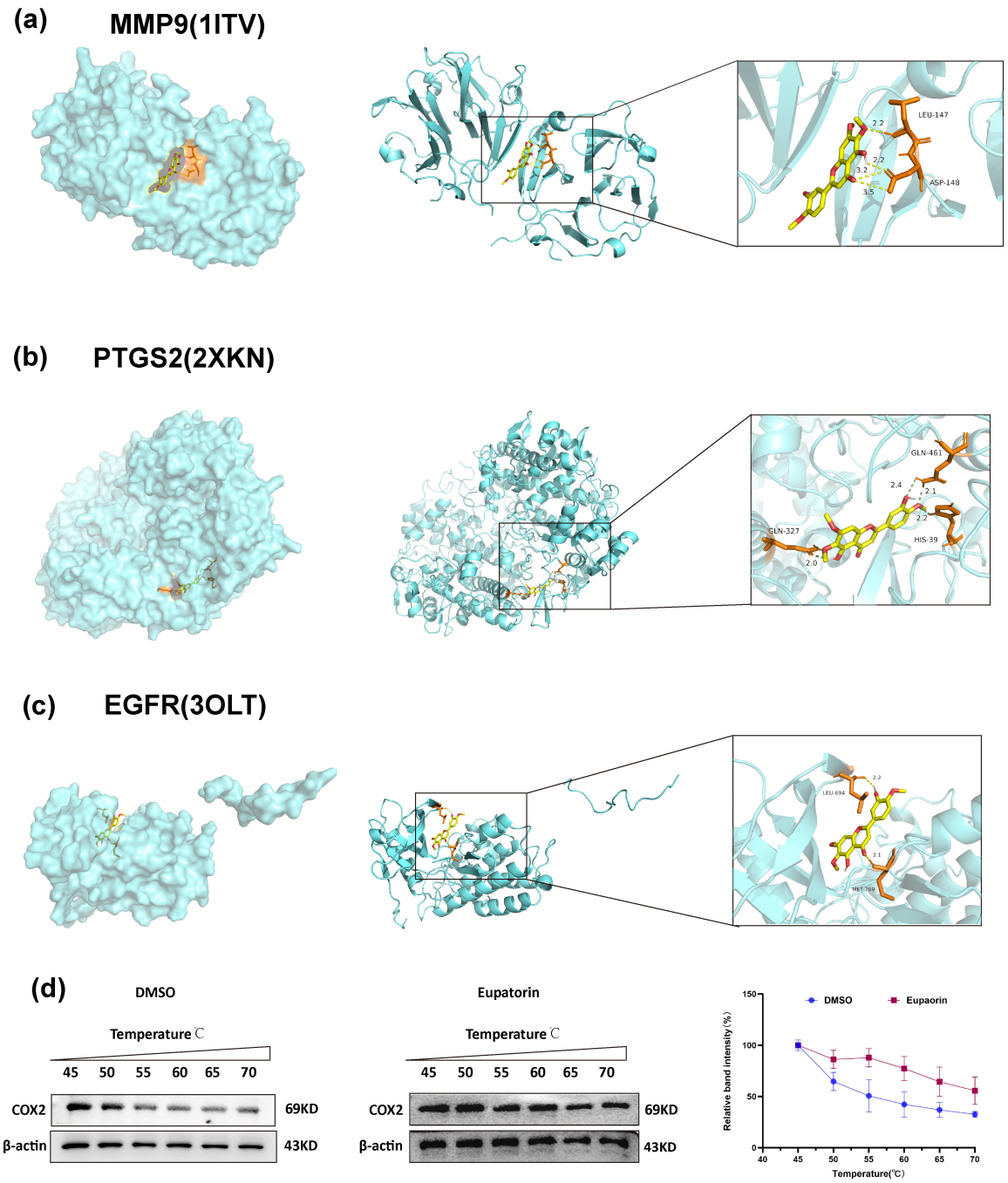


**Fig. 4. Interaction of Eupatorin with three core targets.** (a) MMP9–Eupatorin. (b) PTGS2–Eupatorin. (c) EGFR–Eupatorin. The left figure represents the atom binding diagram of a molecule and protein. The middle figure represents the overall binding pattern between the two, and the right figure shows an enlarged view of the molecule and protein binding, where the text indicates the residue name. The yellow dashed lines indicate hydrogen bonds. (d) Eupatorin protected the COX2 protein against temperature-dependent degeneration in chondrocytes. The values are presented as the means ± SD (n = 3).

**Table 3. Binding energies of the compound and hub targets (kcal/mol).**

| NO. | Receptors | PDB ID | Binding Energy (kcal/mol) | Centre | | | Size | | |
|---|---|---|---|---|---|---|---|---|---|
| | | | | X | Y | Z | X | Y | Z |
| 1 | MMP9 | 1ITV | –7.5 | –27.68 | –40.35 | –15.84 | 68 | 60 | 46 |
| 2 | EGFR | 2XKN | –7.8 | 6.17 | 7.48 | 57.74 | 90 | 62 | 46 |
| 3 | PTGS2 | 3OLT | –9.4 | 23.52 | 41.69 | 39.61 | 70 | 80 | 92 |

(20 μM) to systematically evaluate the effects of Eupatorin. EdU staining indicated that Eupatorin inhibited the proliferation of IL-1$\beta$-stimulated chondrocytes (Fig. 5c). Further analysis of cell cycle regulatory markers, including proliferating cell nuclear antigen (PCNA) and minichromosome maintenance 2 (MCM2), demonstrated that Eupatorin dose-dependently suppressed their expression in IL-1$\beta$-stimulated chondrocytes (Fig. 5d).

IF staining revealed a dose-dependent reduction in MMP13 expression in response to 5–20 μM Eupatorin (Fig. 6a). To evaluate the regulatory effect of IL-1$\beta$ on inflammatory mediators, we analysed the mRNA expression of key proinflammatory molecules: interleukin-1$\beta$ (*IL-1*$\beta$), C-X-C chemokine ligand 3 (*CXCL3*), and C-X-C chemokine ligand 6 (*CXCL6*) (Fig. 6b–d). As expected, IL-1$\beta$ treatment significantly elevated the mRNA expression of these three molecules. In contrast, among the non-cytotoxic concentrations of Eupatorin (5–20 μM), Eupatorin mitigated the IL-1$\beta$-triggered inflammatory reaction in chondrocytes, with the maximal inhibitory effect observed at a concentration of 20 μM.

Given that 20 μM Eupatorin had the strongest protective effects on chondrocyte inflammatory responses, extracellular matrix (ECM) damage, and abnormal chondrocyte proliferation without compromising cell viability, this concentration was therefore selected for subsequent investigations.

### *3.3 Eupatorin Inhibits ECM Degradation in IL-1$\beta$-Stimulated Chondrocytes*

The expression of matrix degradation markers (MMP3, MMP13 and MMP9) and matrix synthesis markers (collagen II and ACAN) was evaluated. Immunofluorescence analysis revealed that Eupatorin significantly reduced the protein expression level of MMP3 induced by IL-1$\beta$ (Fig. 7a,b). In addition, Western blot and RT–qPCR analyses revealed that Eupatorin inhibited the expression of MMP3 (Fig. 7c,d) and *MMP9* (Fig. 7e) while upregulating the expression of Collagen II (Fig. 7f,g) and *ACAN* (Fig. 7h). These observations suggest that 20 μM Eupatorin exerts protective effects against IL-1$\beta$-induced chondrocyte injury, possibly by regulating genes involved in ECM degradation and synthesis.

### *3.4 Eupatorin Attenuates Catabolism and Promotes Anabolism in IL-1$\beta$-Stimulated Chondrocytes*

Compared with those in the control group, the protein expression levels of TNF-$\alpha$, IL-1$\beta$, and COX2 in the IL-1$\beta$-stimulated group significantly increased ($p < 0.05$). However, treatment with Eupatorin (20 μM) markedly suppressed the expression of these inflammatory factors ($p < 0.05$), indicating that Eupatorin exerts an anti-inflammatory effect in this pathological context (Fig. 8a–d).

To determine whether Eupatorin also modulates key anabolic regulators in inflamed chondrocytes, we quantified the mRNA levels of *EGFR*, *SOX9* and *KDR* by RT–qPCR. Compared with no treatment, IL-1$\beta$ treatment significantly downregulated the transcription of these genes, whereas treatment with 20 μM Eupatorin partially restored their expression (Fig. 8e–g). These results also suggest that Eupatorin mitigates the IL-1$\beta$-induced imbalance in ECM metabolism in chondrocytes, promoting a more reparative phenotype.

### *3.5 Eupatorin Inhibits IL-1$\beta$-Induced PI3K/AKT Pathway Activation, Downregulates ER-$\alpha$ Expression, and Restores Autophagic Flux*

We investigated the regulatory effects of Eupatorin on the expression of PI3K, AKT, and estrogen receptor $\alpha$ (ER-$\alpha$) in chondrocytes using Western blot analysis. Specifically, we assessed the levels of PI3K and AKT phosphorylation as well as ER-$\alpha$ expression. As shown in Fig. 9a–d, treatment with Eupatorin (20 μM) significantly suppressed the IL-1$\beta$-induced phosphorylation of PI3K and AKT. Additionally, Eupatorin downregulated the expression of ER-$\alpha$.

Given that autophagy is a downstream event of the PI3K/AKT pathway, we therefore examined markers of chondrocyte autophagy. IL-1$\beta$ treatment significantly reduced the LC3-II/I ratio (a marker of autophagosome formation) and increased P62 protein expression (an indicator of impaired autophagic degradation), which is consistent with the blockage of autophagic flux. Notably, treatment with Eupatorin (20 μM) reversed these changes, indicating the recovery of functional autophagy (Fig. 9e–i).

These results indicate that Eupatorin modulates the activity of the PI3K/AKT and estrogen signalling pathways, which may contribute to the functional regulation of chondrocytes.

## 4. Discussion

To investigate the potential mechanisms of Eupatorin in KOA, this study applied a network pharmacology approach, and validated these predictions through molecular docking and *in vitro* experiments. Inflammation and ECM degradation act synergistically to drive cartilage deterioration and pain in KOA [31]. In particular, inflammatory mediators upregulate the expression of matrix-degrading enzymes, such as matrix metalloproteinases (MMPs) and aggrecanase, which cleave collagen and proteoglycans, thus accelerating ECM breakdown [32,33]. Given that articular cartilage lacks vasculature and innervation, its repair capacity is limited, leading to the rapid accumulation of damage [34,35]. As inflammation serves as a key pathogenic driver in KOA, by accelerating the breakdown of the cartilage extracellular matrix and amplifying pain signalling, targeting inflammation is therefore crucial for preserving cartilage structural integrity, halting disease progression, and alleviating clinical symptoms.

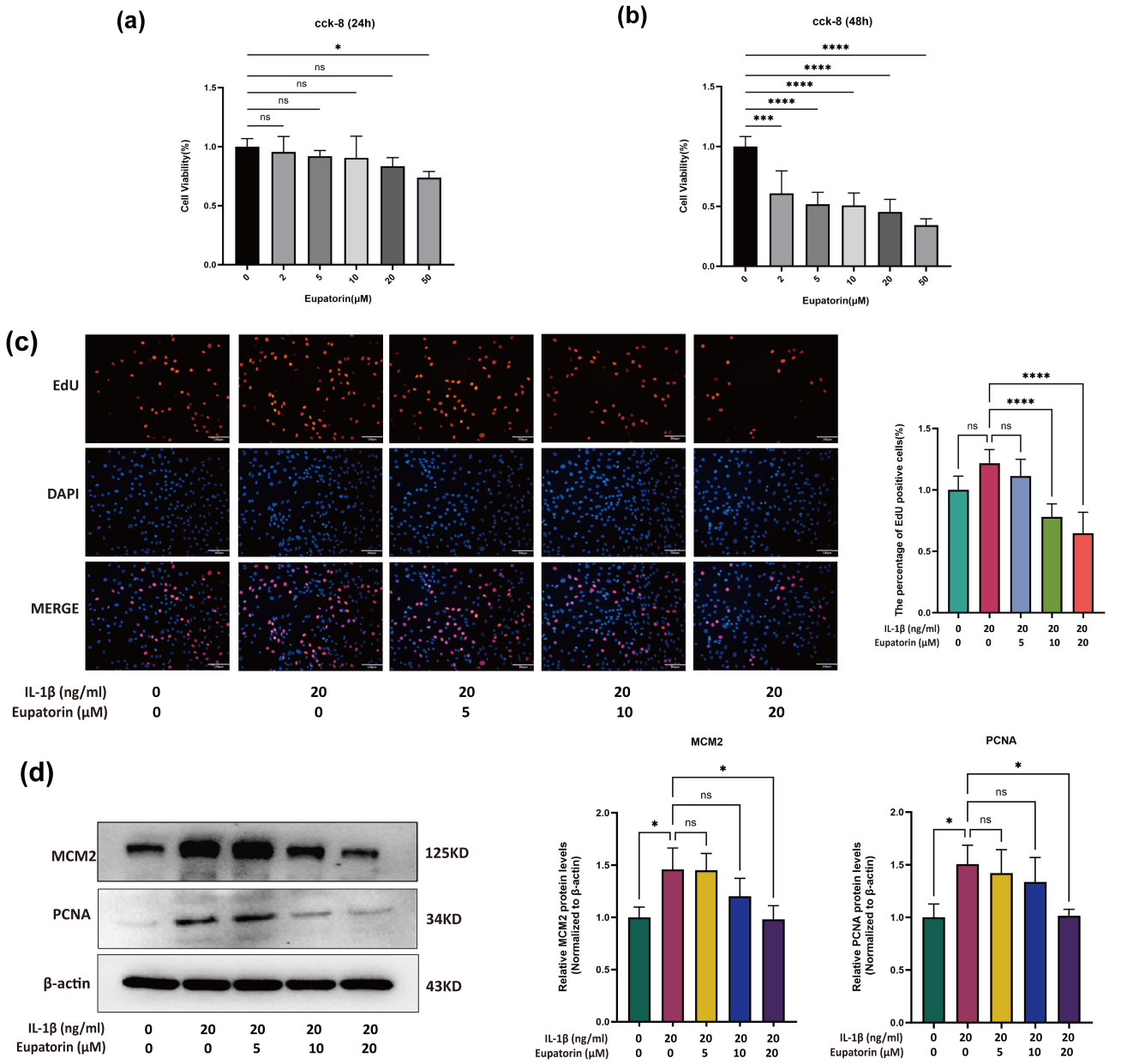


**Fig. 5. Effects of Eupatorin on chondrocyte proliferation.** (a) Chondrocyte viability was measured using the CCK-8 assay after 24 h of incubation with Eupatorin at 2, 5, 10, 20, or 50 μM. (b) Chondrocyte viability was measured using the CCK-8 assay after 48 h of incubation with Eupatorin at 2, 5, 10, 20, or 50 μM. (c) Proliferation of chondrocytes treated with 20 ng/mL IL-1$\beta$ in the absence or presence of 5, 10, or 20 μM Eupatorin for 24 h. The EdU-positive cells are red, while the nuclei are blue. The quantification of the EdU-positive cells is shown on the right; scale bar = 100 μm. (d) The expression levels of MCM2 and PCNA in chondrocytes were detected by Western blotting, with $\beta$-actin serving as the reference. The data are presented as the means ± SD of at least 3 independent biological replicates. Statistical significance among groups is indicated as $p$ values (****$p < 0.0001$, ***$p < 0.001$, *$p < 0.05$, ns: $p > 0.05$), with One-way ANOVA combined with Tukey's post hoc test was utilized to perform multiple group and pairwise comparisons. MCM2, Minichromosome maintenance complex component 2; PCNA, proliferating cell nuclear antigen.

In recent years, natural phytochemicals have been shown to have a protective effect on cartilage tissue [36, 37]. Previous studies have demonstrated the broad pharmacological properties of Eupatorin, especially its anti-inflammatory potential [38,39]. For instance, it has been shown to suppress the lipopolysaccharide (LPS)-induced upregulation of iNOS and COX-2 expression and to exert significant anti-inflammatory effects in carrageenan-induced mouse paw inflammation models [20]. However, its anti-inflammatory roles in the setting of OA remain largely uncharacterized.

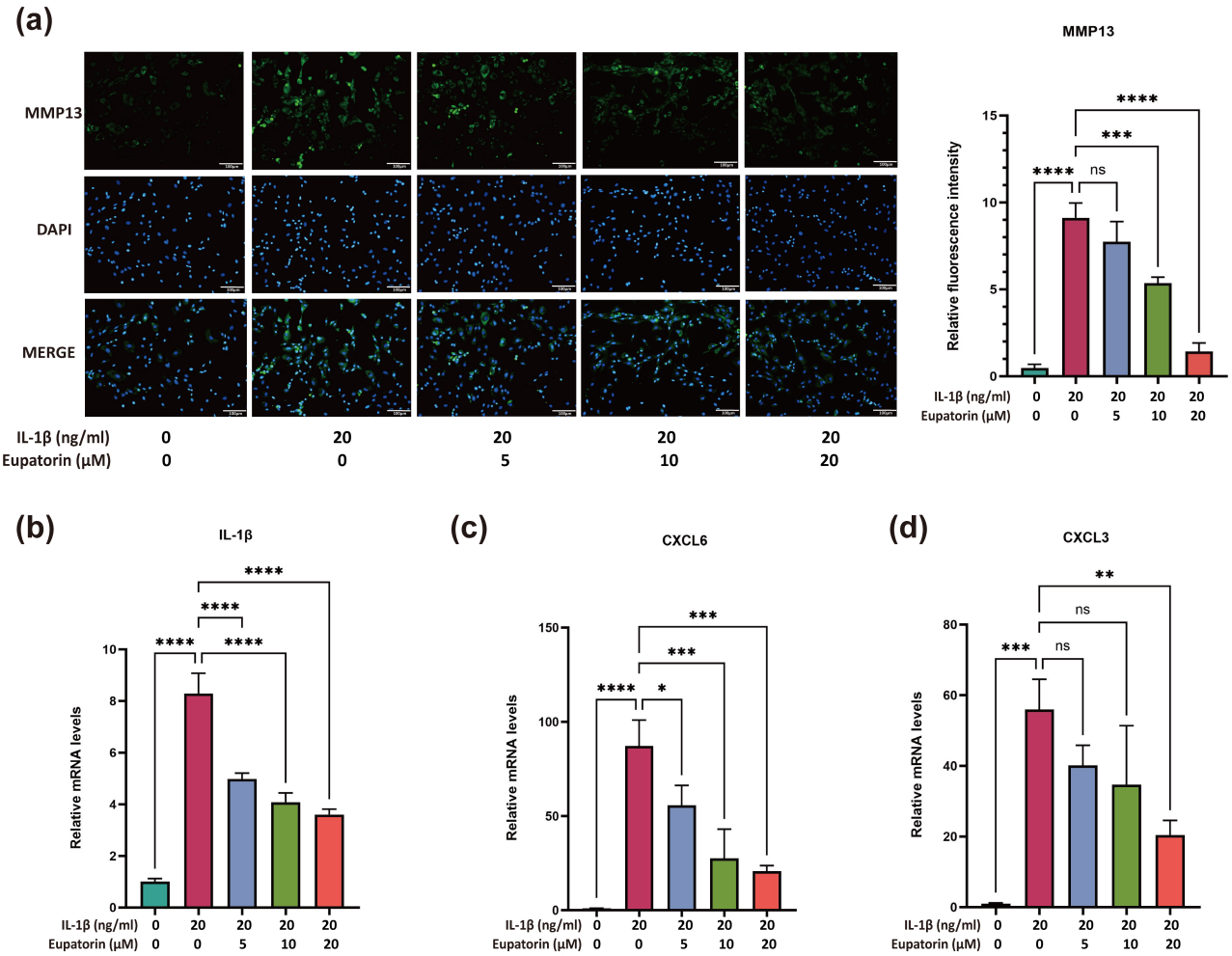


**Fig. 6. Effects of Eupatorin on chondrocyte catabolism and inflammatory responses.** (a) MMP13 expression in IL-1$\beta$-induced chondrocytes following dose-dependent Eupatorin intervention and quantification of fluorescence intensity; scale bar = 100 μm (n = 6). (b) The mRNA levels of *IL-1β* were determined using RT–qPCR. (c) The mRNA levels of *CXCL6* were determined using RT–qPCR. (d) The mRNA levels of *CXCL3* were determined using RT–qPCR. The data are presented as the means ± SD of at least 3 independent biological replicates. Statistical significance among groups is indicated as $p$ values (****$p < 0.0001$, ***$p < 0.001$, **$p < 0.01$, *$p < 0.05$, ns: $p > 0.05$), with One-way ANOVA combined with Tukey's post hoc test was utilized to perform multiple group and pairwise comparisons. MMP13, Matrix Metallopeptidase 13; IL-1$\beta$, Interleukin-1$\beta$; CXCL6, C-X-C motif chemokine ligand 6; CXCL3, C-X-C motif chemokine ligand 3.

In the present study, network pharmacology analysis demonstrated that Eupatorin shares multiple targets with KOA, highlighting several genes closely related to inflammation and extracellular matrix remodelling. Among them, PTGS2, MMP9, and EGFR emerged as pivotal nodes in the PPI network. Molecular docking further supported their potential relevance by demonstrating favourable binding affinities with Eupatorin. Our findings indicate that Eupatorin exhibit protective effects against IL-1$\beta$-induced damage in chondrocytes through the modulation of inflammatory signalling pathways and matrix degradation processes. PTGS2 (COX2) is a critical enzyme that drives the production of prostaglandin E2 and other eicosanoids, thus amplifying inflammatory cascades and enhancing the expression levels of cartilage matrix-degrading enzymes such as MMPs [40,41]. In particular, MMP9 plays a central role in cartilage catabolism by cleaving essential extracellular matrix components [42]. In contrast, EGFR has been reported to exert chondroprotective effects by maintaining tissue homeostasis and suppressing catabolic responses, as evidenced by the rapid development of KOA in EGFR-deficient *mice* and the downregulation of EGFR expression under inflammatory stimulation [43]. Furthermore, our study demonstrated that IL-1$\beta$ decreases the expression of KDR (also known as VEGFR2, the fourth most important hub gene) in chondrocytes, which is reversed by Eupatorin. Since VEGFR2 is localized in hypertrophic cartilage, this phenomenon may result from short-term IL-1$\beta$ stimulation of differentiated chondrocytes, and its reliability requires confirmation through *in vivo* validation [44–46]. Our

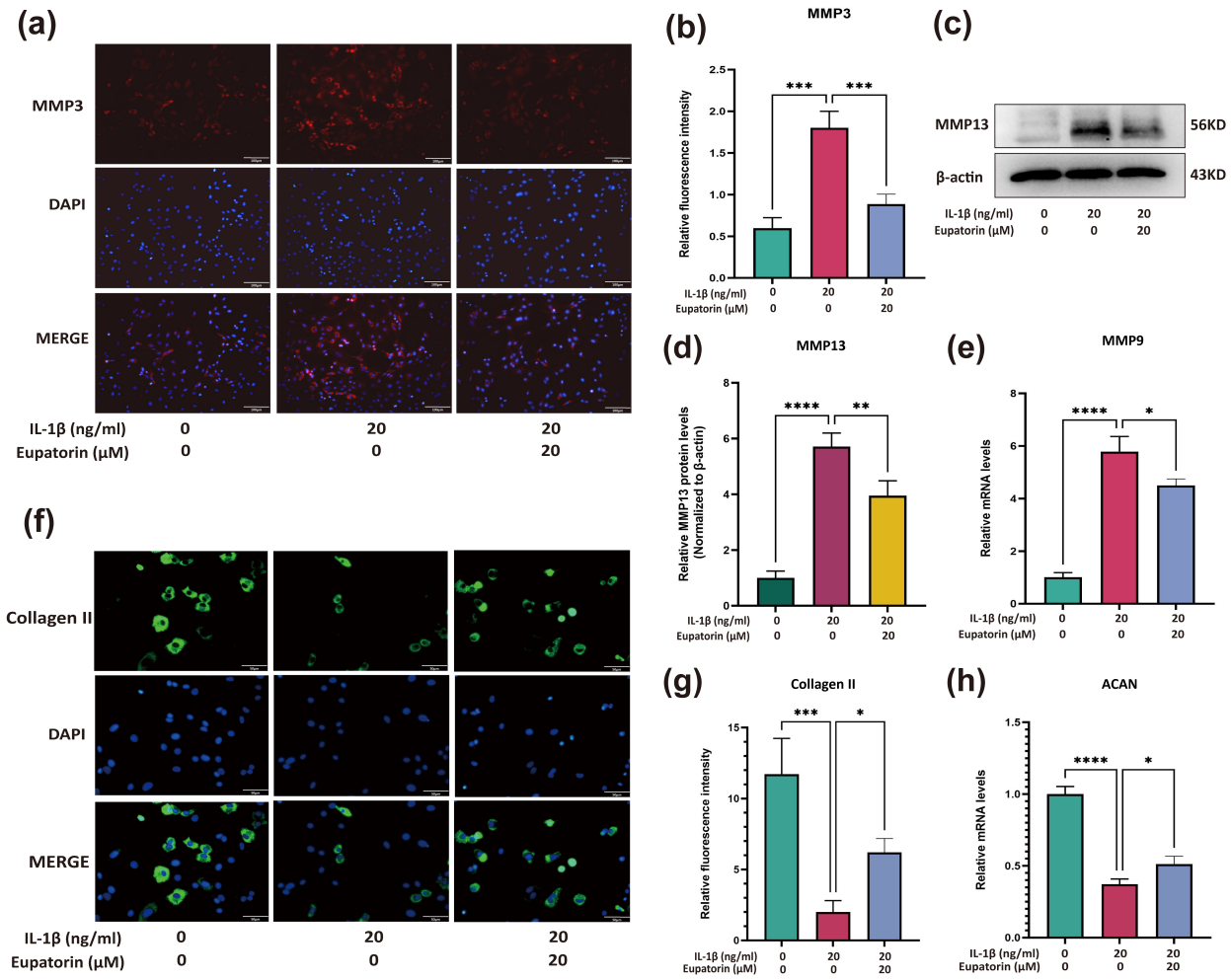


**Fig. 7. Eupatorin attenuates ECM breakdown in IL-1$\beta$-stimulated chondrocytes**. (a) Immunofluorescence staining of the MMP3 protein in chondrocytes. The red signal represents MMP3; scale bar: 100 μm (n = 6). (b) Quantification of the fluorescence intensity of the MMP3 protein. (c) MMP13 expression in Eupatorin (20 μM)-treated chondrocytes in the presence of IL-1$\beta$. (d) Results from the quantitative analysis of the expression of MMP13. (e) The mRNA expression levels of *MMP9* were determined by RT–qPCR. (f) Immunofluorescence staining of the Collagen II protein in chondrocytes. The green signal represents Collagen II; scale bar: 50 μm (n = 6). (g) Quantification of the collagen II protein fluorescence intensity. (h) The mRNA expression levels of *ACAN* were determined by RT–qPCR. Relative fluorescence intensity was quantified using ImageJ software. The data are presented as the means ± SD of more than or equal to 3 independent experimental biological replicates. Statistical significance among groups is indicated by $p$ values (****$p < 0.0001$, ***$p < 0.001$, **$p < 0.01$, *$p < 0.05$), with One-way ANOVA combined with Tukey's post hoc test was utilized to perform multiple group and pairwise comparisons. MMP13, Matrix Metallopeptidase 13; MMP3, Matrix Metallopeptidase 3; MMP9, Matrix Metallopeptidase 9; ACAN, Aggrecan.

findings suggest that Eupatorin may mitigate KOA progression through mechanism: inhibition of COX2- and MMP9-mediated inflammatory and degradative processes while simultaneously preserving EGFR signalling. This regulatory pattern highlights the capacity of Eupatorin to rebalance the disrupted inflammatory–catabolic–protective axis in KOA, thus attenuating cartilage destruction.

For a deeper exploration of the underlying mechanisms of Eupatorin's protective role in KOA, we performed GO and KEGG enrichment analyses, and the findings revealed its involvement in pathways associated with inflammatory regulation and extracellular matrix degradation. These processes are central to KOA pathogenesis, as proinflammatory cytokines such as IL-1$\beta$ disrupt cartilage homeostasis and drive chondrocyte-mediated catabolic activity [47,48]. Eupatorin activity appears to be mitigated by dampening cytokine production, which is consistent with previous works that have shown that Eupatorin reduces the levels of NO, TNF-$\alpha$, and IL-6 in RAW 264.7 cells exposed to LPS [19,49]. Our findings extend this anti-inflammatory profile to chondrocytes, indicating that Eupatorin may attenuate IL-1$\beta$-induced inflammatory responses. By mod-

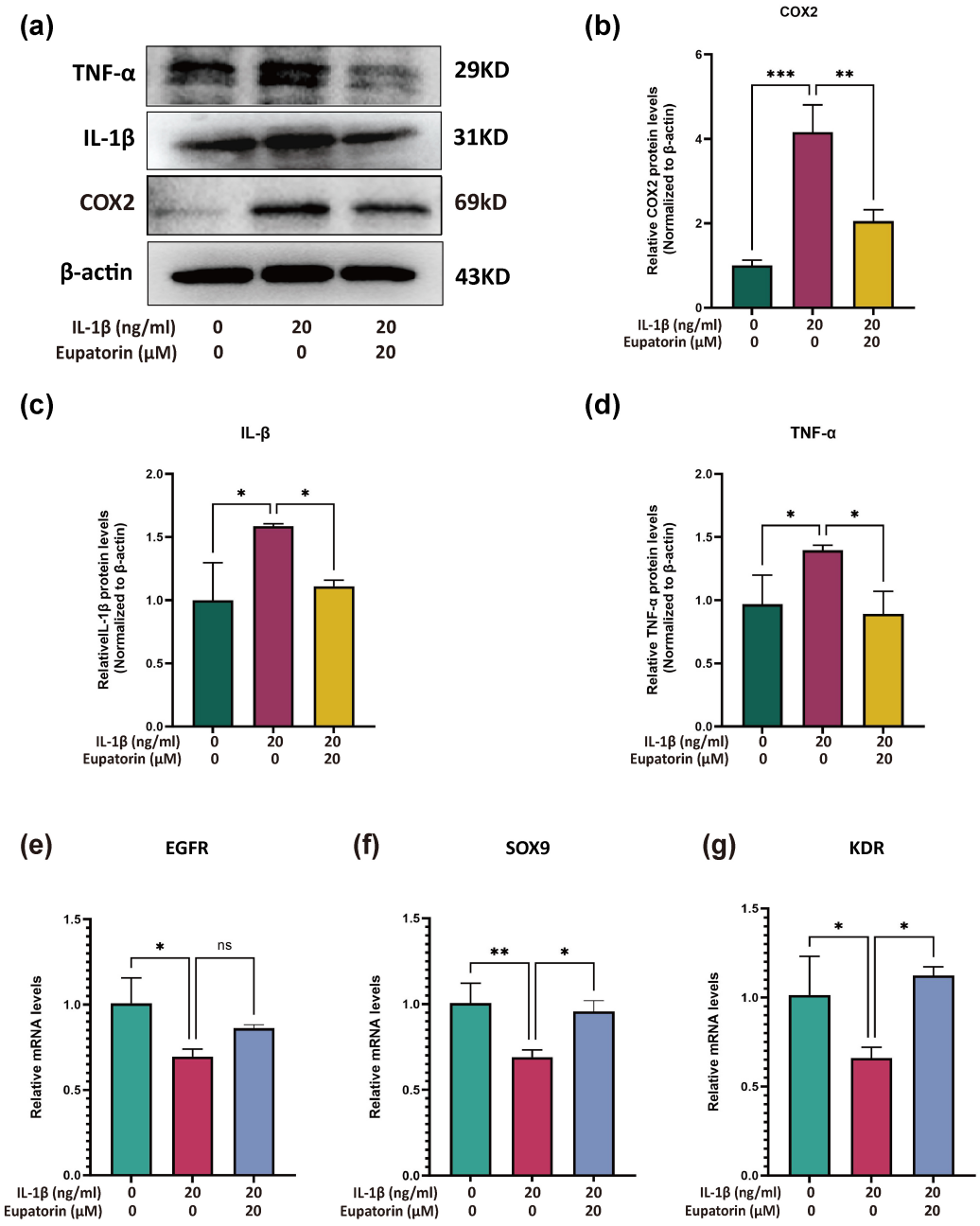


**Fig. 8. Effects of Eupatorin on IL-1$\beta$-stimulated chondrocytes.** (a) The effects of Eupatorin on the expressions of TNF-$\alpha$, IL-1$\beta$, and COX2 in IL-1$\beta$-stimulated chondrocytes were investigated. (b) Results from the quantitative analysis of COX2 expression. (c) Quantitative analysis of the expression of IL-1$\beta$. (d) Quantitative analysis of the expression of TNF-$\alpha$. (e) The mRNA levels of *EGFR* were determined using RT–qPCR. (f) The mRNA levels of *SOX9* were determined using RT–qPCR. (g) The mRNA levels of *KDR* were determined using RT–qPCR. The data are presented as the means $\pm$ SD of more than or equal to 3 independent experimental biological replicates. Statistical significance among groups is indicated as $p$ values (***$p < 0.001$, **$p < 0.01$, *$p < 0.05$, ns: $p > 0.05$). One-way ANOVA combined with Tukey's post hoc test was utilized to perform multiple group and pairwise comparisons. TNF-$\alpha$, tumour necrosis factor-alpha; IL-1$\beta$, interleukin 1 beta; COX2, cyclooxygenase-2.

ulating both inflammatory mediators and catabolic pathways, Eupatorin appears to restore a more balanced chondrocyte phenotype, thus contributing to the preservation of cartilage integrity in KOA. Notably, healthy chondrocytes, which lack vascular nutrition, maintain a relatively low proliferation rate. In contrast, KOA chondrocytes, perturbed by inflammatory factors, exhibit enhanced catabolic activity accompanied by increased proliferation [50–52]. The anti-proliferative effect of Eupatorin observed in the EdU assay (Fig. 5c) may represent a response to the IL-

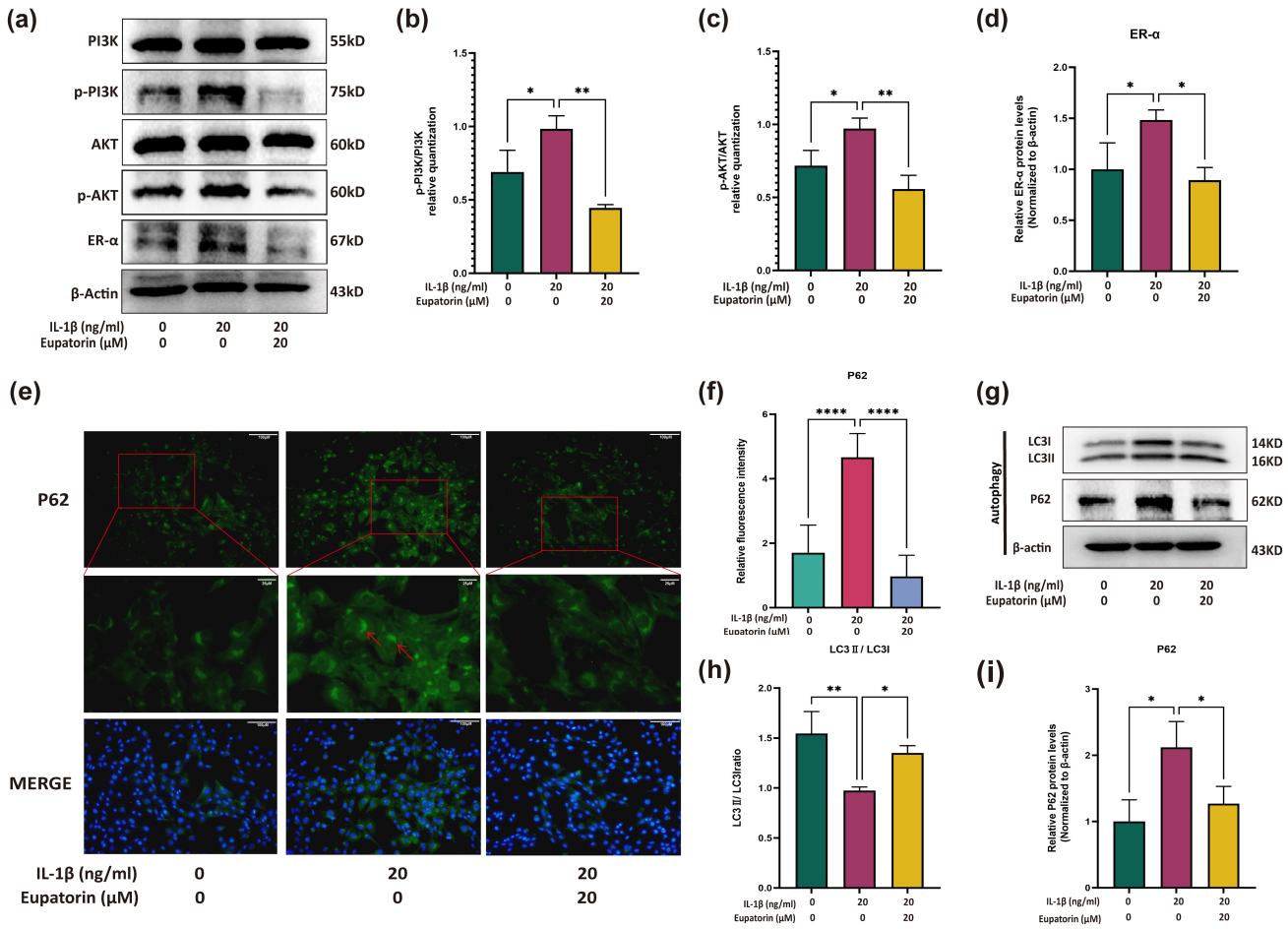


**Fig. 9. Regulatory effects of Eupatorin on PI3K/AKT, the estrogen signalling pathway, and autophagy-related proteins.** (a) Expression of the PI3K, AKT, p-PI3K, p-AKT and ER-$\alpha$ proteins. (b) Results from the quantitative analysis of p-PI3K/PI3K expression. (c) Results from the quantitative analysis of p-AKT/AKT expression. (d) Quantitative analysis of ER-$\alpha$ expression. (e) Immunofluorescence staining of the P62 protein in chondrocytes. The green signal represents P62 localized in cytoplasmic bodies (red arrows); scale bars: 100 μm and 25 μm (magnified) (n = 6). (f) Quantification of P62 protein fluorescence intensity. (g) Expression of the LC3 and P62 proteins. (h) Quantitative analysis of the expression of LC3 II/I. (i) Quantitative analysis of P62 expression. The data are presented as the means ± SD of more than or equal to 3 independent experimental biological replicates. Statistical significance among groups is indicated as $p$ values (****$p < 0.0001$, **$p < 0.01$, *$p < 0.05$). One-way ANOVA combined with Tukey's post hoc test was utilized to perform multiple group and pairwise comparisons. PI3K, phosphatidylinositol 3-kinase; AKT, protein kinase B; LC3, microtubule-associated protein 1 light chain 3; P62, sequestosome 1.

1$\beta$-induced aberrant chondrocyte clustering associated with early KOA pathogenesis in primary chondrocytes.

From another perspective, KEGG analysis revealed that the PI3K-AKT pathway was the Greatest enrichment magnitude and that the estrogen signalling pathway was the most significantly enriched. Estrogen and its receptors are widely expressed in joint-resident cells, suggesting that joint tissues are responsive to estrogenic regulation [53]. ER-$\alpha$, in particular, is known to regulate estrogen-responsive genes and contribute to bone and cartilage homeostasis [54]. Nevertheless, the role of estrogen in KOA remains controversial. While some studies indicate protective effects, others report that excessive estrogen signalling may exacerbate joint degeneration by enhancing proteoglycan loss and MMP production under inflammatory conditions [55,56]. In this context, our findings imply that Eupatorin may help rebalance estrogen signalling by limiting ER-$\alpha$ overactivation during inflammation, thus contributing to the preservation of the cartilage matrix. This regulatory action aligns with its broader anti-inflammatory and anti-catabolic profile, further supporting the therapeutic potential of Eupatorin in KOA.

It is well known that estrogen can exert biological effects through both classical genomic and nongenomic signalling pathways [57]. Among these, the activation of nongenomic signalling pathways involves various protein and lipid kinases, including PI3K/AKT [58,59]. ER-$\alpha$ can directly interact with PI3K, thus triggering down-

stream AKT signalling, which is closely linked to KOA progression through the regulation of chondrocyte survival, inflammatory responses, extracellular matrix metabolism, and MMP expression [60,61]. Notably, in the PI3K/AKT pathway, upon binding to ligands such as EGF or TGF-$\alpha$, EGFR is activated and recruits the PI3K catalytic subunit, thereby initiating the phosphorylation-dependent upregulation of the PI3K/AKT pathway [62]. Once activated, the PI3K/AKT pathway promotes COX2 expression to exacerbate cartilage inflammation and upregulate MMP9 to accelerate cartilage destruction by activating downstream transcription factors (e.g., NF-$\kappa$B), and pharmacological inhibition of this pathway has been shown to alleviate OA-related pathological processes [63–65].

In chondrocytes, inflammation and oxidative stress often coexist and collectively disrupt the balance of chondrocyte autophagy [66]; notably, the PI3K/AKT pathway functions as a pivotal regulator of chondrocyte autophagy, a conserved cellular process essential for maintaining intracellular homeostasis [67]. In the context of KOA, excessive PI3K/AKT activation further impairs chondrocyte autophagy through the phosphorylation and activation of mammalian target of rapamycin (mTOR), thus inducing a "damage overload" state within chondrocytes [68,69]. In the present study, Eupatorin modulated autophagy activation, as indicated by reduced P62 expression and an elevated LC3II/LC3I ratio (Fig. 9e–i); however, our results revealed no statistically significant effect of Eupatorin on chondrocyte senescence (**Supplementary Fig. 2**). This observation aligns with the notion that chondrocyte senescence is typically a late-stage consequence of prolonged autophagy impairment rather than an immediate response to autophagy-related changes [70]. Alternatively, the regulatory effect of Eupatorin may be restricted to the autophagic process itself, without extending to the subsequent senescence pathway. Thus, more systematic studies are needed to confirm this. Within this context, we found that Eupatorin may exert protective actions, at least in part, by modulating PI3K/AKT activity, thus attenuating inflammatory and catabolic signalling while promoting chondrocyte autophagy in KOA.

Taken together, these findings strengthen the validity of network pharmacology predictions and highlight Eupatorin as a potential therapeutic candidate for KOA. Notably, Eupatorin is a bioactive flavonoid predominantly isolated from plants of the Eupatorium genus, which have been documented to exert potential therapeutic effects on chronic inflammatory diseases [71,72]. Furthermore, given that KOA is recognized as a local inflammatory disease, leveraging well-established nanocarrier-based drug delivery strategies for flavonoids may enable targeted drug accumulation in joint tissues, enhance therapeutic efficacy, and reduce systemic risks [73,74], thereby underscoring considerable clinical value that warrants further exploration. Nonetheless, a number of limitations are worth noting. The current analysis relied primarily on existing databases and published literature, which may introduce biases related to data quality and completeness. More importantly, as a network pharmacology-based analysis, it is inherently characterized by predictivity rather than practical verification. Moreover, it overlooks the dynamic microenvironment of organisms, such as differences in cell types and tissue specificity, which may lead to deviations between predictions and actual biological effects. Mechanistic evidence relies primarily on changes in key phosphorylation nodes; subsequent validation with activator intervention experiments is needed. Furthermore, we recognize that Eupatorin, as a natural flavonoid, exhibits polypharmacological characteristics and may engage with multiple signalling pathways beyond our initial hypotheses. While our study focused on the PI3K/AKT and estrogen signalling pathways, we cannot definitively exclude contributions from other enriched pathways to the effects of Eupatorin. Our experiments provide foundational insights into the regulation of chondrocytes by Eupatorin, yet KOA involves chronic, multifactorial inflammation, cartilage degradation, and systemic immune crosstalk [75], a complexity not fully captured by the high-dose IL-1$\beta$ *in vitro* model used here.

This represents a key limitation, as our data do not rule out off-target interactions or unexplored pathway involvement. To address these limitations, future studies will incorporate expanded phosphoproteomic profiling to determine Eupatorin's activation of distinct pathways in KOA. Additionally, investigations will prioritize KOA-relevant cell types, including synovial fibroblasts and macrophages, alongside multicellular co-culture models, to fully elucidate its integrated biological effects within the disease context. Additionally, more clinically relevant models, such as medial meniscus destabilization (DMM) in rodents, should be adopted to better mimic KOA progression.

## 5. Conclusion

In conclusion, network pharmacology analysis, molecular docking and experimental validation suggest that Eupatorin may exert chondroprotective effects by regulating the activity of the PI3K/AKT and estrogen signalling pathways to modulate downstream inflammation and autophagy, but this pathway dependency requires further confirmation. These findings offer preliminary insights for subsequent studies exploring its role in KOA.

## Availability of Data and Materials

The datasets generated and analyzed during the current study are available from the corresponding author upon reasonable request.

## Author Contributions

MJZ; JLY: study design, data acquisition and statistical analysis, cell-based experiments, drafting of the original

manuscript. JHL; YSG; CMH: database searching, visualization of the main results. TTM; YQZ; XHH; LLC; JWD: supplementary data collection, figure preparation, supplementary data analysis, manuscript revision. XBW; DFD: conception, research framework design, critical review of key results, final manuscript review and approval. All authors contributed to editorial changes in the manuscript. All authors read and approved the final manuscript. All authors have participated sufficiently in the work and agreed to be accountable for all aspects of the work.

## Ethics Approval and Consent to Participate

The study was conducted in compliance with the laboratory animal guideline for ethical review of animal welfare and approved by Ethics Committee of Shanghai University of Traditional Chinese Medicine (PZSHUTCM2311290001).


## Acknowledgment

Not applicable.

## Funding

This study was supported by the National Natural Science Foundation of China (grant numbers 81902306); Shanghai Municipal Health Commission Traditional Chinese Medicine Research Project (grant numbers 2024QN012).


## Conflict of Interest

The authors declare no conflict of interest.

## Supplementary Material

Supplementary material associated with this article can be found, in the online version, at https://doi.org/10.31083/FBL46747.

## References


[1] Poole AR. Osteoarthritis as a whole joint disease. HSS Journal: the Musculoskeletal Journal of Hospital for Special Surgery. 2012; 8: 4–6. https://doi.org/10.1007/s11420-011-9248-6.

[2] Pettenuzzo S, Berardo A, Belluzzi E, Pozzuoli A, Ruggieri P, Carniel EL, *et al*. Mechanical insights into fat pads: a comparative study of infrapatellar and suprapatellar fat pads in osteoarthritis. Connective Tissue Research. 2025; 66: 272–283. https://doi.org/10.1080/03008207.2025.2502591.

[3] Olansen J, Dyke JP, Aaron RK. Is Osteoarthritis a Vascular Disease? Frontiers in Bioscience (Landmark Edition). 2024; 29: 113. https://doi.org/10.31083/j.fbl2903113.

[4] Yao Q, Wu X, Tao C, Gong W, Chen M, Qu M, *et al*. Osteoarthritis: pathogenic signaling pathways and therapeutic targets. Signal Transduction and Targeted Therapy. 2023; 8: 56. https://doi.org/10.1038/s41392-023-01330-w.

[5] Jang S, Lee K, Ju JH. Recent Updates of Diagnosis, Pathophysiology, and Treatment on Osteoarthritis of the Knee. International Journal of Molecular Sciences. 2021; 22: 2619. https://doi.org/10.3390/ijms22052619.

[6] Brophy RH, Fillingham YA. AAOS Clinical Practice Guideline Summary: Management of Osteoarthritis of the Knee (Nonarthroplasty), Third Edition. The Journal of the American Academy of Orthopaedic Surgeons. 2022; 30: e721–e729. https://doi.org/10.5435/JAAOS-D-21-01233.

[7] Chen X, Zheng J, Yin L, Li Y, Liu H. Transplantation of three mesenchymal stem cells for knee osteoarthritis, which cell and type are more beneficial? a systematic review and network meta-analysis. Journal of Orthopaedic Surgery and Research. 2024; 19: 366. https://doi.org/10.1186/s13018-024-04846-1.

[8] Santamaria S, Cuffaro D, Nuti E, Ciccone L, Tuccinardi T, Liva F, *et al*. Exosite inhibition of ADAMTS-5 by a glycoconjugated arylsulfonamide. Scientific Reports. 2021; 11: 949. https://doi.org/10.1038/s41598-020-80294-1.

[9] Brebion F, Gosmini R, Deprez P, Varin M, Peixoto C, Alvey L, *et al*. Discovery of GLPG1972/S201086, a Potent, Selective, and Orally Bioavailable ADAMTS-5 Inhibitor for the Treatment of Osteoarthritis. Journal of Medicinal Chemistry. 2021; 64: 2937–2952. https://doi.org/10.1021/acs.jmedchem.0c02008.

[10] Breland AN, Ross MK, Fitzkee NC, Elder SH. In Silico Insights into the Inhibition of ADAMTS-5 by Punicalagin and Ellagic Acid for the Treatment of Osteoarthritis. International Journal of Molecular Sciences. 2025; 26: 4093. https://doi.org/10.3390/ijms26094093.

[11] Courties A, Kouki I, Soliman N, Mathieu S, Sellam J. Osteoarthritis year in review 2024: Epidemiology and therapy. Osteoarthritis and Cartilage. 2024; 32: 1397–1404. https://doi.org/10.1016/j.joca.2024.07.014.

[12] Hunter DJ, Bierma-Zeinstra S. Osteoarthritis. Lancet (London, England). 2019; 393: 1745–1759. https://doi.org/10.1016/S0140-6736(19)30417-9.

[13] Fujii Y, Liu L, Yagasaki L, Inotsume M, Chiba T, Asahara H. Cartilage Homeostasis and Osteoarthritis. International Journal of Molecular Sciences. 2022; 23: 6316. https://doi.org/10.3390/ijms23116316.

[14] Kapoor M, Martel-Pelletier J, Lajeunesse D, Pelletier JP, Fahmi H. Role of proinflammatory cytokines in the pathophysiology of osteoarthritis. Nature Reviews. Rheumatology. 2011; 7: 33–42. https://doi.org/10.1038/nrrheum.2010.196.

[15] Clockaerts S, Bastiaansen-Jenniskens YM, Feijt C, De Clerck L, Verhaar JAN, Zuurmond AM, *et al*. Cytokine production by infrapatellar fat pad can be stimulated by interleukin 1$\beta$ and inhibited by peroxisome proliferator activated receptor $\alpha$ agonist. Annals of the Rheumatic Diseases. 2012; 71: 1012–1018. https://doi.org/10.1136/annrheumdis-2011-200688.

[16] Zhou F, Mei J, Han X, Li H, Yang S, Wang M, *et al*. Kinsenoside attenuates osteoarthritis by repolarizing macrophages through inactivating NF-$\kappa$B/MAPK signaling and protecting chondrocytes. Acta Pharmaceutica Sinica. B. 2019; 9: 973–985. https://doi.org/10.1016/j.apsb.2019.01.015.

[17] He L, Pan Y, Yu J, Wang B, Dai G, Ying X. Decursin alleviates the aggravation of osteoarthritis via inhibiting PI3K-Akt and NF-kB signal pathway. International Immunopharmacology. 2021; 97: 107657. https://doi.org/10.1016/j.intimp.2021.107657.

[18] Chriscensia E, Arham AA, Wibowo EC, Gracius L, Nathanael J, Hartrianti P. Eupatorin from Orthosiphon aristatus: A Review of The Botanical Origin, Pharmacological Effects and Isolation Methods. Current Bioactive Compounds. 2023; 19: 45–60. /https://doi.org/10.2174/1573407219666230331122318.

[19] Lu J, Alarifi S, Ahamed A, Wang R. Eupatorin Mitigates Airway Inflammation in Ovalbumin-Induced Allergic Asthma in Mice by Regulating Th2 Cytokines and Oxidative Stress. Journal of Biochemical and Molecular Toxicology. 2025; 39: e70219. https://doi.org/10.1002/jbt.70219.

[20] Laavola M, Nieminen R, Yam MF, Sadikun A, Asmawi MZ, Basir R, *et al*. Flavonoids eupatorin and sinensetin present in Orthosiphon stamineus leaves inhibit inflammatory gene expres-

sion and STAT1 activation. Planta Medica. 2012; 78: 779–786. https://doi.org/10.1055/s-0031-1298458.

[21] Abd Razak N, Yeap SK, Alitheen NB, Ho WY, Yong CY, Tan SW, *et al*. Eupatorin Suppressed Tumor Progression and Enhanced Immunity in a 4T1 Murine Breast Cancer Model. Integrative Cancer Therapies. 2020; 19: 1534735420935625. https://doi.org/10.1177/1534735420935625.

[22] González-Cortazar M, Salinas-Sánchez DO, Herrera-Ruiz M, Román-Ramos DC, Zamilpa A, Jiménez-Ferrer E, *et al*. Eupatorin and Salviandulin-A, with Antimicrobial and Anti-Inflammatory Effects from *Salvia lavanduloides* Kunth Leaves. Plants (Basel, Switzerland). 2022; 11: 1739. https://doi.org/10.3390/plants11131739.

[23] Zhang R, Zhu X, Bai H, Ning K. Network Pharmacology Databases for Traditional Chinese Medicine: Review and Assessment. Frontiers in Pharmacology. 2019; 10: 123. https://doi: 10.3389/fphar.2019.00123.

[24] Kim S. Getting the most out of PubChem for virtual screening. Expert Opinion on Drug Discovery. 2016; 11: 843–855. https://doi.org/10.1080/17460441.2016.1216967.

[25] Daina A, Michielin O, Zoete V. SwissTargetPrediction: updated data and new features for efficient prediction of protein targets of small molecules. Nucleic Acids Research. 2019; 47: W357–W364. https://doi.org/10.1093/nar/gkz382.

[26] Xie Y, Qin X, Zhou T, Zhou Y, Tang L, Wang J, *et al*. Investigating the protective effect of loganin in ovariectomy induced bone loss through network pharmacology and molecular docking. Experimental and Therapeutic Medicine. 2024; 28: 417. https://doi.org/10.3892/etm.2024.12706.

[27] Tang Y, Li M, Wang J, Pan Y, Wu FX. CytoNCA: a cytoscape plugin for centrality analysis and evaluation of protein interaction networks. Bio Systems. 2015; 127: 67–72. https://doi.org/10.1016/j.biosystems.2014.11.005.

[28] Chin CH, Chen SH, Wu HH, Ho CW, Ko MT, Lin CY. cytoHubba: identifying hub objects and sub-networks from complex interactome. BMC Systems Biology. 2014; 8 Suppl 4: S11. https://doi.org/10.1186/1752-0509-8-S4-S11.

[29] Yu G, Wang LG, Han Y, He QY. clusterProfiler: an R package for comparing biological themes among gene clusters. Omics: a Journal of Integrative Biology. 2012; 16: 284–287. https://doi.org/10.1089/omi.2011.0118.

[30] Wang C, Liu X, Guo S. Network pharmacology-based strategy to investigate the effect and mechanism of $\alpha$-solanine against glioma. BMC Complementary Medicine and Therapies. 2023; 23: 371. https://doi.org/10.1186/s12906-023-04215-1.

[31] Zhang J, Li K, Qiu X. Exploring causal correlations between inflammatory cytokines and knee osteoarthritis: a two-sample Mendelian randomization. Frontiers in Immunology. 2024; 15: 1362012. https://doi.org/10.3389/fimmu.2024.1362012.

[32] Chow YY, Chin KY. The Role of Inflammation in the Pathogenesis of Osteoarthritis. Mediators of Inflammation. 2020; 2020: 8293921. https://doi.org/10.1155/2020/8293921.

[33] Chan CM, Macdonald CD, Litherland GJ, Wilkinson DJ, Skelton A, Europe-Finner GN, *et al*. Cytokine-induced MMP13 Expression in Human Chondrocytes Is Dependent on Activating Transcription Factor 3 (ATF3) Regulation. The Journal of Biological Chemistry. 2017; 292: 1625–1636. https://doi.org/10.1074/jbc.M116.756601.

[34] Robinson WH, Lepus CM, Wang Q, Raghu H, Mao R, Lindstrom TM, *et al*. Low-grade inflammation as a key mediator of the pathogenesis of osteoarthritis. Nature Reviews. Rheumatology. 2016; 12: 580–592. https://doi.org/10.1038/nrrheum.2016.136.

[35] Xu W, Zhu J, Hu J, Xiao L. Engineering the biomechanical microenvironment of chondrocytes towards articular cartilage tissue engineering. Life Sciences. 2022; 309: 121043. https://doi.org/10.1016/j.lfs.2022.121043.

[36] Pérez-Lozano ML, Cesaro A, Mazor M, Esteve E, Berteina-Raboin S, Best TM, *et al*. Emerging Natural-Product-Based Treatments for the Management of Osteoarthritis. Antioxidants (Basel, Switzerland). 2021; 10: 265. https://doi.org/10.3390/antiox10020265.

[37] Lee YT, Yunus MHM, Ugusman A, Yazid MD. Natural Compounds Affecting Inflammatory Pathways of Osteoarthritis. Antioxidants (Basel, Switzerland). 2022; 11: 1722. https://doi.org/10.3390/antiox11091722.

[38] Yam MF, Tew WY, Tan CS, Qiu Q, Zhou R, Wang X, *et al*. Investigation of synergistic interaction of sinensetin, eupatorin, and 3'-hydroxy-5,6,7,4'-tetramethoxyflavone in vasodilation efficacy. Hypertension Research: Official Journal of the Japanese Society of Hypertension. 2024; 47: 3193–3199. https://doi.org/10.1038/s41440-024-01907-0.

[39] Akram M, Syed AS, Kim KA, Lee JS, Chang SY, Kim CY, *et al.* Heme oxygenase 1-mediated novel anti-inflammatory activities of Salvia plebeia and its active components. Journal of Ethnopharmacology. 2015; 174: 322–30. https://doi.org/10.1016/j.jep.2015.08.028.

[40] Nakata K, Hanai T, Take Y, Osada T, Tsuchiya T, Shima D, *et al*. Disease-modifying effects of COX-2 selective inhibitors and non-selective NSAIDs in osteoarthritis: a systematic review. Osteoarthritis and Cartilage. 2018; 26: 1263–1273. https://doi.org/10.1016/j.joca.2018.05.021.

[41] Tu M, Yang M, Yu N, Zhen G, Wan M, Liu W, *et al*. Inhibition of cyclooxygenase-2 activity in subchondral bone modifies a subtype of osteoarthritis. Bone Research. 2019; 7: 29. https://doi.org/10.1038/s41413-019-0071-x.

[42] Teunissen van Manen IJ, van Kooten NJT, Di Ceglie I, Theeuwes WF, Jimenez-Royo P, Cleveland M, *et al*. Identification of CD64 as a marker for the destructive potential of synovitis in osteoarthritis. Rheumatology (Oxford, England). 2024; 63: 1180–1188. https://doi.org/10.1093/rheumatology/kead314.

[43] Wei Y, Ma X, Sun H, Gui T, Li J, Yao L, *et al*. EGFR Signaling Is Required for Maintaining Adult Cartilage Homeostasis and Attenuating Osteoarthritis Progression. Journal of Bone and Mineral Research: the Official Journal of the American Society for Bone and Mineral Research. 2022; 37: 1012–1023. https://doi.org/10.1002/jbmr.4531.

[44] Horváth E, Sólyom Á, Székely J, Nagy EE, Popoviciu H. Inflammatory and Metabolic Signaling Interfaces of the Hypertrophic and Senescent Chondrocyte Phenotypes Associated with Osteoarthritis. International Journal of Molecular Sciences. 2023; 24: 16468. https://doi.org/10.3390/ijms242216468.

[45] Gerber HP, Vu TH, Ryan AM, Kowalski J, Werb Z, Ferrara N. VEGF couples hypertrophic cartilage remodeling, ossification and angiogenesis during endochondral bone formation. Nature Medicine. 1999; 5: 623–628. https://doi.org/10.1038/9467.

[46] Honorati MC, Cattini L, Facchini A. IL-17, IL-1beta and TNF-alpha stimulate VEGF production by dedifferentiated chondrocytes. Osteoarthritis and Cartilage. 2004; 12: 683–691. https://doi.org/10.1016/j.joca.2004.05.009.

[47] Koyama T, Uchida K, Fukushima K, Ohashi Y, Uchiyama K, Inoue G, *et al*. Elevated levels of TNF-$\alpha$, IL-1$\beta$ and IL-6 in the synovial tissue of patients with labral tear: a comparative study with hip osteoarthritis. BMC Musculoskeletal Disorders. 2021; 22: 33. https://doi.org/10.1186/s12891-020-03888-w.

[48] Cardoso JM, Ribeiro AC, Botelho J, Proença L, Noronha S, Alves RC. The Influence of Genetic Polymorphisms on the Expression of Interleukin-1beta, Prostaglandin E2 and Tumor Necrosis Factor Alpha in Peri-Implant Crevicular Fluid: A Cross-Sectional Study. International Journal of Molecular Sciences. 2024; 25: 651. https://doi.org/10.3390/ijms25010651.

[49] González-Chávez MM, Ramos-Velázquez CS, Serrano-Vega

R, Pérez-González C, Sánchez-Mendoza E, Pérez-Gutiérrez S. Anti-inflammatory activity of standardized dichloromethane extract of Salvia connivens on macrophages stimulated by LPS. Pharmaceutical Biology. 2017; 55: 1467–1472. https://doi.org/10.1080/13880209.2017.1305423.

[50] Ding DF, Xue Y, Zhang JP, Zhang ZQ, Li WY, Cao YL, *et al*. Similarities and differences between rat and mouse chondrocyte gene expression induced by IL-1$\beta$. Journal of Orthopaedic Surgery and Research. 2022; 17: 70. https://doi.org/10.1186/s13018-021-02889-2.

[51] Varela-Eirin M, Loureiro J, Fonseca E, Corrochano S, Caeiro JR, Collado M, *et al*. Cartilage regeneration and ageing: Targeting cellular plasticity in osteoarthritis. Ageing Research Reviews. 2018; 42: 56–71. https://doi.org/10.1016/j.arr.2017.12.006.

[52] Simsa-Maziel S, Monsonego-Ornan E. Interleukin-1$\beta$ promotes proliferation and inhibits differentiation of chondrocytes through a mechanism involving down-regulation of FGFR-3 and p21. Endocrinology. 2012; 153: 2296–2310. https://doi.org/10.1210/en.2011-1756.

[53] Tang J, Liu T, Wen X, Zhou Z, Yan J, Gao J, *et al*. Estrogen-related receptors: novel potential regulators of osteoarthritis pathogenesis. Molecular Medicine (Cambridge, Mass.). 2021; 27: 5. https://doi.org/10.1186/s10020-021-00270-x.

[54] Wang N, Zhang X, Rothrauff BB, Fritch MR, Chang A, He Y, *et al*. Novel role of estrogen receptor-$\alpha$ on regulating chondrocyte phenotype and response to mechanical loading. Osteoarthritis and Cartilage. 2022; 30: 302–314. https://doi.org/10.1016/j.joca.2021.11.002.

[55] Martín-Millán M, Castañeda S. Estrogens, osteoarthritis and inflammation. Joint Bone Spine. 2013; 80: 368–373. https://doi.org/10.1016/j.jbspin.2012.11.008.

[56] Son YO, Park S, Kwak JS, Won Y, Choi WS, Rhee J, *et al*. Estrogen-related receptor $\gamma$ causes osteoarthritis by upregulating extracellular matrix-degrading enzymes. Nature Communications. 2017; 8: 2133. https://doi.org/10.1038/s41467-017-01868-8.

[57] Chakrabarti S, Morton JS, Davidge ST. Mechanisms of estrogen effects on the endothelium: an overview. The Canadian Journal of Cardiology. 2014; 30: 705–712. https://doi.org/10.1016/j.cjca.2013.08.006.

[58] Gui Z, Shi W, Zhou F, Yan Y, Li Y, Xu Y. The role of estrogen receptors in intracellular estrogen signaling pathways, an overview. The Journal of Steroid Biochemistry and Molecular Biology. 2025; 245: 106632. https://doi.org/10.1016/j.jsbmb.2024.106632.

[59] Wang N, Lu Y, Rothrauff BB, Zheng A, Lamb A, Yan Y, *et al*. Mechanotransduction pathways in articular chondrocytes and the emerging role of estrogen receptor-$\alpha$. Bone Research. 2023; 11: 13. https://doi.org/10.1038/s41413-023-00248-x.

[60] Xue JF, Shi ZM, Zou J, Li XL. Inhibition of PI3K/AKT/mTOR signaling pathway promotes autophagy of articular chondrocytes and attenuates inflammatory response in rats with osteoarthritis. Biomedicine & Pharmacotherapy. 2017; 89: 1252–1261. https://doi.org/10.1016/j.biopha.2017.01.130.

[61] Sun K, Luo J, Guo J, Yao X, Jing X, Guo F. The PI3K/AKT/mTOR signaling pathway in osteoarthritis: a narrative review. Osteoarthritis and Cartilage. 2020; 28: 400–409. https://doi.org/10.1016/j.joca.2020.02.027.

[62] Chen XC, Wei XT, Guan JH, Shu H, Chen D. EGF stimulates glioblastoma metastasis by induction of matrix metalloproteinase-9 in an EGFR-dependent mechanism. Oncotarget. 2017; 8: 65969–65982. https://doi.org/10.18632/oncotarget.19622.

[63] Han G, Zhang Y, Li H. The Combination Treatment of Curcumin and Probucol Protects Chondrocytes from TNF-$\alpha$ Induced Inflammation by Enhancing Autophagy and Reducing Apoptosis via the PI3K-Akt-mTOR Pathway. Oxidative Medicine and Cellular Longevity. 2021; 2021: 5558066. https://doi.org/10.1155/2021/5558066.

[64] Li J, Jiang M, Yu Z, Xiong C, Pan J, Cai Z, *et al*. Artemisinin relieves osteoarthritis by activating mitochondrial autophagy through reducing TNFSF11 expression and inhibiting PI3K/AKT/mTOR signaling in cartilage. Cellular & Molecular Biology Letters. 2022; 27: 62. https://doi.org/10.1186/s11658-022-00365-1.

[65] Qu Y, Shen Y, Teng L, Huang Y, Yang Y, Jian X, *et al*. Chicoric acid attenuates tumor necrosis factor-$\alpha$-induced inflammation and apoptosis via the Nrf2/HO-1, PI3K/AKT and NF-κB signaling pathways in C28/I2 cells and ameliorates the progression of osteoarthritis in a rat model. International Immunopharmacology. 2022; 111: 109129. https://doi.org/10.1016/j.intimp.2022.109129.

[66] Yang K, Zhang H, Luo Y, Zhang J, Wang M, Liao P, *et al*. Gypenoside XVII Prevents Atherosclerosis by Attenuating Endothelial Apoptosis and Oxidative Stress: Insight into the ER$\alpha$-Mediated PI3K/Akt Pathway. International Journal of Molecular Sciences. 2017; 18: 77. https://doi.org/10.3390/ijms18020077.

[67] Zhu C, Zhang L, Ding X, Wu W, Zou J. Non-coding RNAs as regulators of autophagy in chondrocytes: Mechanisms and implications for osteoarthritis. Ageing Research Reviews. 2024; 99: 102404. https://doi.org/10.1016/j.arr.2024.102404.

[68] Lou L, Zhu Z, Xu L, Wu Z, Wang X, Yuan L, *et al*. Glabridin mitigates osteoarthritis progression through modulation of the PI3K/AKT/FOXO3A autophagy axis. Phytomedicine: International Journal of Phytotherapy and Phytopharmacology. 2025; 148: 157359. https://doi.org/10.1016/j.phymed.2025.157359.

[69] Ma L, Zhang R, Li D, Qiao T, Guo X. Fluoride regulates chondrocyte proliferation and autophagy via PI3K/AKT/mTOR signaling pathway. Chemico-biological Interactions. 2021; 349: 109659. https://doi.org/10.1016/j.cbi.2021.109659.

[70] Huang J, Wu L, Zhao Y, Zhao H. Programmed Cell Death of Chondrocytes, Synovial Cells, Osteoclasts, and Subchondral Bone Cells in Osteoarthritis. Journal of Inflammation Research. 2025; 18: 12323–12360. https://doi.org/10.2147/JIR.S514309.

[71] Hussain Y, Mathur A, Meena A, Luqman S. Eupatorin: A comprehensive review of its pharmacological activities and underlying molecular mechanisms. European Journal of Pharmacology. 2025; 1008: 178330. https://doi.org/10.1016/j.ejphar.2025.178330.

[72] Gu G, Ahn S, Lim SJ, Paek JH, Kim S, Lim SS, *et al*. Eupatorium japonicum extract regulates inflammation through suppression of the TRIF-dependent signaling pathway of toll-like receptors. Food Science and Biotechnology. 2014; 23: 587–592. http://doi.org/10.1007/s10068-014-0080-x.

[73] Gan K, Li J, Zhang X, Feng Z, Liu J, Zhao F. MXene-Mediated Nanocarrier Delivery Enhances the Chondroprotective Effects of Quercetin in Experimental Osteoarthritis. International Journal of Nanomedicine. 2025; 20: 11553–11567. https://doi.org/10.2147/IJN.S540035.

[74] De Roover A, Escribano-Núñez A, Monteagudo S, Lories R. Fundamentals of osteoarthritis: Inflammatory mediators in osteoarthritis. Osteoarthritis and Cartilage. 2023; 31: 1303–1311. https://doi.org/10.1016/j.joca.2023.06.005.

[75] Hashimoto K, Oda Y, Nakagawa K, Ikeda T, Ohtani K, Akagi M. LOX-1 deficient mice show resistance to zymosan-induced arthritis. European Journal of Histochemistry: EJH. 2018; 62: 2847. https://doi.org/10.4081/ejh.2018.2847.